

1 **Projected Changes and Time of Emergence of Temperature Extremes over Australia**
2 **in CMIP5 and CMIP6**

3
4 **Xu Deng^{1,2*} and Sarah E. Perkins-Kirkpatrick^{1,2}**

5 ¹School of Science, University of New South Wales, Canberra, ACT, Australia.

6 ²ARC Centre of Excellence for Climate Extremes, University of New South Wales, Canberra,
7 ACT, Australia.

8
9 Corresponding author: Xu Deng (xu.deng@student.adfa.edu.au)

10
11
12 **Key Points:**

- 13 • There indicates a “warm-get-warmer” pattern for some extremes over Australia and
14 tropical regions usually show the highest warming
- 15 • Compared to CMIP5, the higher warming for some extremes in CMIP6 can lead to earlier
16 time of emergence under the highest scenario
- 17 • Internal variability influences the determination of the noise
18

19 Abstract

20 This study focuses on the projections and time of emergence (TOE) for temperature extremes
21 over Australian regions in the phase 6 of Coupled Model Intercomparison Project (CMIP6)
22 models. The model outputs are based on the Shared Socioeconomic Pathways (SSPs) from the
23 Tier 1 experiments (i.e., SSP1-2.6, SSP2-4.5, SSP3-7.0 and SSP5-8.5) in the Scenario Model
24 Intercomparison Project (ScenarioMIP), which is compared with the Representative
25 Concentration Pathways (RCPs) in CMIP5 (i.e., RCP2.6, RCP4.5 and RCP8.5). Furthermore,
26 two large ensembles (LEs) in CMIP6 are used to investigate the effects of internal variability on
27 the projected changes and TOE. As shown in the temporal evolution and spatial distribution, the
28 strongest warming levels are projected under the highest future scenario and the changes for
29 some extremes follow a “warm-get-warmer” pattern over Australia. Over subregions, tropical
30 Australia usually shows the highest warming. Compared to the RCPs in CMIP5, the multi-model
31 medians in SSPs are higher for some indices and commonly exhibit wider spreads, likely related
32 to the different forcings and higher climate sensitivity in a subset of the CMIP6 models. Based
33 on a signal-to-noise framework, we confirm that the emergence patterns differ greatly for
34 different extreme indices and the large uncertainty in TOE can result from the inter-model ranges
35 of both signal and noise, for which internal variability contributes to the determination of the
36 signal. We further demonstrate that the internally-generated variations influence the noise. Our
37 findings can provide useful information for mitigation strategies and adaptation planning over
38 Australia.

39

40 **1 Introduction**

41 Anthropogenic climate change will lead to more severe temperature extremes, which
42 have significant impacts on society and natural systems (Intergovernmental Panel on Climate
43 Change, 2021). To assess possible climate futures, projections by global climate models from the
44 Scenario Model Intercomparison Project (ScenarioMIP; O'Neill et al., 2016) as part of the
45 Coupled Model Intercomparison Project phase 6 (CMIP6; Eyring et al., 2016) are useful
46 resources, and may provide new insights into how temperature extremes are projected to change
47 under climate change (e.g., Alexander & Arblaster, 2017; Grose et al., 2020; Sillmann, Kharin,
48 Zwiers, et al., 2013; Thibeault & Seth, 2014).

49 Over Australia, Alexander and Arblaster (2017) indicated that significant increases
50 (decreases) are projected for the occurrence of warm (cold) extremes by the end of this century
51 under the intermediate- and highest-emission scenarios in CMIP5, and that these changes are
52 most distinct in the tropics. Compared to 29 CMIP5 models, Grose et al. (2020) documented that
53 projected changes in temperature extremes over Australia are more distinct and span narrower
54 ranges in seven CMIP6 models. However, the smaller number of models used in this study may
55 lead to misleading conclusions. Recently, Tebaldi et al. (2021) demonstrated that the CMIP6
56 ensemble projects higher warming and larger spread for global mean temperature compared with
57 CMIP5, which could result from both a wider range of radiative forcing and higher climate
58 sensitivity in a subset of CMIP6 models. In the present study, to obtain a more reasonable
59 comparison with CMIP5, more models are included in the CMIP6 ensemble to analyze the
60 projected changes of temperature extremes over Australia.

61 In addition, detecting the time of emergence (TOE) for extremes over Australia needs
62 investigation. TOE is defined as the time when the externally forced climate signal (i.e., forced

63 response) emerges from the noise (i.e., natural variability), suggesting that a significant change is
64 detected and a novel climate regime become evident (e.g., Hawkins et al., 2020; Hawkins &
65 Sutton, 2012; King, Donat, et al., 2015). Estimating TOE can provide insights for mitigation
66 strategies, adaptation planning and scientific community, as the forced response relative to the
67 background noise may be more relevant for the assessment of climate impacts, compared to the
68 absolute change (Beaumont et al., 2011; Deutsch et al., 2008; Hawkins et al., 2020; Hawkins &
69 Sutton, 2012; Ossó et al., 2021). For example, similar absolute changes in extreme temperature
70 can result in different ecological impacts since extratropical ecosystems are usually more
71 resilient than tropical ecosystems, as they are adapted to a more variable climate (Beaumont et
72 al., 2011; Deutsch et al., 2008).

73 Previous studies have concluded that for mean temperature there is earlier TOE over
74 tropical regions than that in the extratropics where the noise is generally larger (e.g., Giorgi &
75 Bi, 2009; Hawkins et al., 2020; Hawkins & Sutton, 2012; Mahlstein et al., 2012; Mahlstein et al.,
76 2011). Furthermore, for warm and cold extremes that display larger variability, the signals for
77 these indices tend to emerge later over both the tropics and extratropics (e.g., King, Donat, et al.,
78 2015; Tan et al., 2018) relative to mean temperature. Currently, most studies on TOE have been
79 conducted at global levels, with less detailed analyses over smaller-scale regions (e.g., Batibeniz
80 et al., 2020; Gaetani et al., 2020; Ossó et al., 2021), especially for Australia (King, Donat, et al.,
81 2015). Under different future scenarios, we aim to investigate the TOE of extreme temperatures
82 over Australia at the subregional scale.

83 A variety of methods have been used in TOE assessment, which can lead to a source of
84 uncertainty (Abatzoglou et al., 2019; Gaetani et al., 2020). A recent study (Gaetani et al., 2020)
85 found that compared to Kolmogorov-Smirnov (KS) non-parametric test (King, Donat, et al.,

86 2015), the signal-to-noise ratio (SNR) frameworks exhibit increased uncertainty and later times
87 for TOE over West Africa (Gaetani et al., 2020). However, the SNR methods facilitate the
88 separation between signal and noise, and identifying both components and their interaction
89 physically (e.g., slow-varying ocean conditions and the modes of internal variability) can deepen
90 our understanding in climate change (e.g., Barnes et al., 2019; Barsugli & Battisti, 1998). In this
91 study, we adopt the method by Hawkins and Sutton (2012) and Hawkins et al. (2020) to address
92 the TOE assessment, which is widely used and allows more cross-study comparisons (e.g.,
93 Abatzoglou et al., 2019; Gaetani et al., 2020; Hawkins et al., 2020; Hawkins & Sutton, 2012;
94 Ossó et al., 2021). For the uncertainty in the detection of TOE in this method, it can arise from
95 inter-model spread not only in the signal, but also from noise (Hawkins & Sutton, 2012).

96 Furthermore, as internal variability can also be an important source of uncertainty for
97 regional climate (Dai & Bloecker, 2019; Deser, Knutti, et al., 2012; Deser, Phillips, et al., 2012;
98 Hawkins & Sutton, 2009; Lehner et al., 2020), single-model initial-condition large ensembles
99 (SMILEs; hereafter LEs) are an important tool to investigate the consequences of the intrinsic
100 variability on the uncertainty in projected changes and TOE of extreme temperatures over
101 Australia, of which external forcing and model structure are identical among the members (e.g.,
102 Dai & Bloecker, 2019; Deser, 2020; Deser et al., 2020; Lehner et al., 2020; Mankin et al., 2020;
103 Perkins-Kirkpatrick et al., 2017; Xie et al., 2015).

104 Previous research evaluated the ability of CMIP6 models to simulate extreme
105 temperatures over Australian regions in the historical period (1950-2014), compared these results
106 to the CMIP5 ensemble, and investigated the effects of internal variability on the corresponding
107 trends based on the LEs in CMIP6 (Deng et al., 2021). Following from this research, the
108 purposes of this study are: to assess future climate changes of the extremes and the TOE over

109 Australian regions in both the CMIP6 and CMIP5 models, and to explore the effects of internal
110 variability on the projected changes and TOE based on LEs in CMIP6.

111

112 **2 Data and Methods**

113 2.1 Model Data

114 Although the scenarios in the ScenarioMIP consist of two tiers, we only use the Tier 1
115 experiments based on the Shared Socioeconomic Pathway (SSP) scenarios: SSP1-2.6, SSP2-4.5,
116 SSP3-7.0 and SSP5-8.5, as these sample a varying range of possible emission futures and contain
117 relatively large number of model outputs. Among them, SSP1-2.6, SSP2-4.5 and SSP5-8.5
118 indicate the same nominal stratospheric-adjusted radiative forcing (2.6, 4.5 and 8.5 W m⁻²)
119 reached in 2100, compared to the scenarios based on Representative Concentration Pathways
120 (RCPs) used in CMIP5 (i.e., RCP2.6, RCP4.5 and RCP8.5); and SSP3-7.0 fills a gap between
121 medium and high end in the range of future forcing pathways, not included in previous CMIP
122 generations (O'Neill et al., 2016; Tebaldi et al., 2021). Despite the similarity among the future
123 scenarios in CMIP6 and CMIP5, it is noted that there are some differences, such as the
124 composition of some radiatively active gases or species (e.g., CO₂ and CH₄) and aerosol
125 emissions, making the resulting effective radiative forcing (ERF) different (Lurton et al., 2020;
126 Riahi et al., 2017; Tebaldi et al., 2021).

127 As one aim of this study is to compare the two CMIP ensembles in projected changes and
128 TOE in extremes, we do not consider the interdependence among the models and use emergent
129 constraints or any other ways of model weighting to reduce the differences between CMIP6 and
130 CMIP5 (e.g., Tokarska et al., 2020), which is similar to the practice by Seneviratne and Hauser

131 (2020). Similar to Deng et al. (2021), only one ensemble member (typically the first member) in
132 each model is considered for the main part of analysis. There are 25 models in CMIP6 and 26
133 models in CMIP5 for at least one of the future scenarios. In addition, two LEs under SSP5-8.5
134 and SSP1-2.6 in CMIP6 are used to investigate the impacts of internal variability on the
135 projected changes and TOE of the extremes: CanESM5-LE and MIROC6-LE, which contain 25
136 members and 50 members, respectively. Detailed information on the simulations from CMIP6
137 and CMIP5 models are listed in the Tables S1 and S2, respectively.

138 2.2 Temperature indices

139 As in Deng et al. (2021), based on daily maximum and minimum temperatures (TX and
140 TN), the annualized temperature extremes defined by the Expert Team on Climate Change
141 Detection and Indices (ETCCDI; Zhang et al., 2011) are used, which forms a continuous and
142 comprehensive investigation of changes in extremes, similar to other studies for CMIP5 (e.g.,
143 Alexander & Arblaster, 2017; Sillmann, Kharin, Zhang, et al., 2013; Sillmann, Kharin, Zwiers, et
144 al., 2013; Thibeault & Seth, 2014). Besides diurnal temperature range (DTR), other extreme
145 indices for temperatures are classified into four categories: absolute indices (hottest day [TXx],
146 coldest day [TXn], warmest night [TNx] and coldest night [TNn]), threshold indices (summer
147 days [SU], tropical nights [TR] and frost days [FD]), percentile-based indices (warm days
148 [TX90p], cold days [TX10p], warm nights [TN90p] and cold nights [TN10p]), and duration
149 indices (warm spell duration index [WSDI] and cold spell duration index [CSDI]). The bootstrap
150 resampling procedure by Zhang et al. (2005) is applied to the percentile-based and duration
151 indices, among which the spells crossing year boundaries are taken into consideration for WSDI
152 and CSDI. Since the definitions of growing season length (GSL) and ice days (ID) are not

153 suitable over most of Australia (Alexander & Arblaster, 2017), we do not use them in this study.
154 Detailed information on the indices can be found in Table S3.

155 2.3 Time of Emergence

156 The TOE is determined using the signal-to-noise framework as detailed by Hawkins and
157 Sutton (2012) and Hawkins et al. (2020), which is considered as the first year when the signal-to-
158 noise ratio (SNR) is larger than nominated thresholds (e.g., 1 and 2). As suggested by Frame et
159 al. (2017), we consider SNR=1 as the threshold for an “unusual” climate and SNR=2 as
160 “unfamiliar”. This approach linearly regresses annual local variations in temperature extremes
161 onto global mean surface temperature change ($\Delta GMST$), relative to the base period:

$$162 \hat{L}(t) = \alpha G(t) + \beta$$

163 where $\hat{L}(t)$ represents the regressed $L(t)$, denoting annual local changes in extremes over time;
164 $G(t)$ is a smoothed version of $\Delta GMST$ over the same period; α defines the linear scaling between
165 $\hat{L}(t)$ and $G(t)$; and β is a constant. $\Delta GMST$ is smoothed with a “Locally Weighted Scatterplot
166 Smoothing” filter (LOWESS; Cleveland, 1979) of 21 years, which filters out interannual
167 variability (though retaining multi-decadal variability). The signal of local climate change
168 described by $\Delta GMST$ is $\alpha G(t)$, and the noise is defined as the standard deviation of the residuals
169 ($L(t) - \alpha G(t)$). The method implies that local variations for some variables scale well with
170 $\Delta GMST$ (Fischer et al., 2014; Seneviratne & Hauser, 2020; Sutton et al., 2015). It is also noted
171 that internal variability can contribute to the determination of signal, which may introduce
172 further uncertainty in the estimate of TOE (Gaetani et al., 2020; Kumar & Ganguly, 2018;
173 Lehner et al., 2020).

174 To compare observed SNR with the simulations, Berkeley Earth Surface Temperatures
175 (BEST; Rohde, Muller, Jacobsen, Muller, et al., 2013; Rohde, Muller, Jacobsen, Perlmutter, et
176 al., 2013) is used in this study. Although TN in BEST is biased over Australia (Deng et al.,
177 2021), the TX and TN in BEST show higher correlation compared to Australian gridded climate
178 data (AGCD, previously termed Australian Water Availability Project [AWAP]; Jones et al.,
179 2009), which is better than other global datasets, including National Centers for Environmental
180 Prediction/National Center for Atmospheric Research (NCEP/NCAR) Reanalysis 1 (NCEP1;
181 Kalnay et al., 1996), NCEP/Department of Energy (DOE) Reanalysis 2 (NCEP2; Kanamitsu et
182 al., 2002), Twentieth Century Reanalysis (20CR; Compo et al., 2011), and European Centre for
183 Medium-Range Weather Forecasts (ECMWF) Reanalysis version 5 (ERA5) with preliminary
184 extension to 1950 (Bell et al., 2021; Hersbach et al., 2020) (not shown).

185 2.4 Regional Assessment

186 According to climatological and geographical conditions (Perkins et al., 2014;
187 http://www.bom.gov.au/climate/change/about/temp_timeseries.shtml), Australia is divided into
188 nine sub-regions: AUS (Australia), NA (Northern Australia), SA (Southern Australia), SEA
189 (South East Australia), MEA (Middle Eastern Australia), TA (Tropical Australia), SWA (South
190 West Australia), SSA (Southern South Australia), CAU (Central Australia), and MWA (Mid-
191 Western Australia), shown in Table S4 and Fig. S1, which allows a detailed assessment over
192 smaller subregions. And the base period is from 1961 to 1990, which is commonly used and
193 allows us to analyze TOE with respect to a recent period. Still, we regrid TX and TN to $1^\circ \times 1^\circ$
194 resolution using bilinear interpolation, and then calculate extreme indices. In addition, grid boxes
195 containing less than 75% land are masked out (King, van Oldenborgh, et al., 2015).

196 In the next section, temporal variations from 1950 to 2100 for the ETCCDI indices in
197 different future scenarios are first analyzed, followed by the spatial patterns of the changes in the
198 indices over 2071-2011 and 2031-2060. Then, the SNR and TOE for TXx and TNn is calculated
199 to address when a novel climate for temperature extremes emerges. For consistency among
200 CMIP6, CMIP5 and BEST, we calculate the noise in SNR for the period 1950-2005, as the
201 estimation of noise can stabilize over longer timescale (Dai & Bloecker, 2019; Santer et al.,
202 2011). Finally, we use two LEs to check the effects of internal variability on the projected
203 responses of extremes and TOE.

204

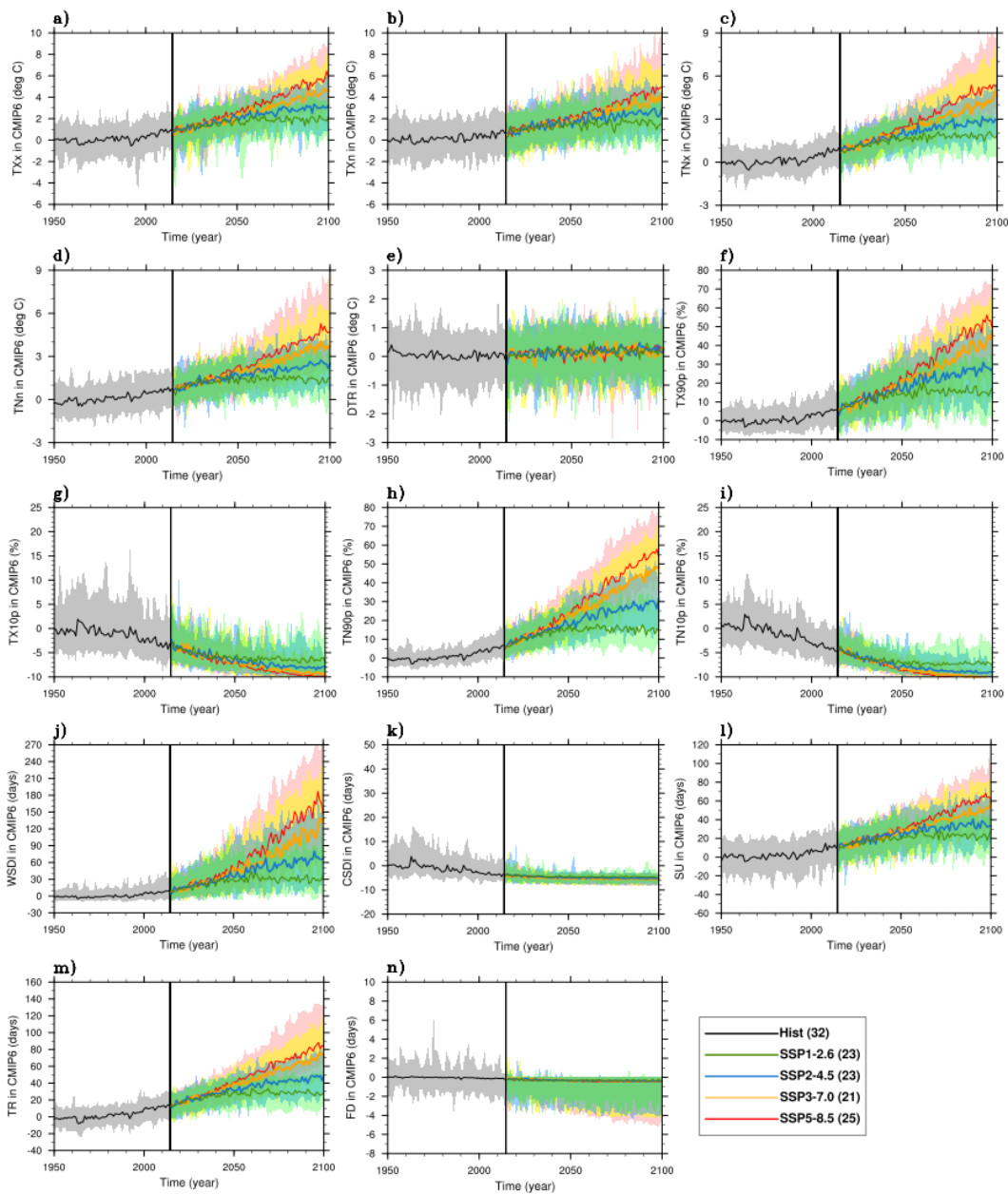
205 **3 Results**

206 **3.1 Projected changes**

207 Relative to the base period 1961-1990, Figs. 1 and 2 indicate time series of the anomalies
208 for the 14 ETCCDI indices averaged over Australia (10-45°S, 110-155°E) during the period
209 1950-2100 under different future scenarios in CMIP6 (SSP1-2.6, SSP2-4.5, SSP3-7.0 and SSP5-
210 8.5) and CMIP5 (RCP2.6, RCP4.5 and RCP8.5). For the multi-model medians (Fig. 1),
211 consistent with RCPs in CMIP5 (Fig. 2), the Tier 1 experiments in ScenarioMIP show projected
212 increases in the absolute indices (TXx, TXn, TNx and TNn) and in the warm extremes for
213 percentile-based, duration and threshold indices (TX90p, TN90p, WSDI, SU and TR); in
214 contrast, there are decreases in other cold extremes (TX10p, TN10p, CSDI and FD).

215 Among the scenarios, the indices under SSP5-8.5 and RCP8.5 generally show larger
216 warming evolution, especially by the end of the century. Moreover, except for DTR, CSDI and
217 FD (Fig. 1e, k and n), extremes under the SSP3-7.0 fill the gap between SSP2-4.5&RCP4.5 and

218 SSP5-8.5&RCP8.5. For example, in the year 2100, the median of TXx under SSP3-7.0 is
219 4.58°C, lower than 5.78°C&5.82°C in SSP5-8.5&RCP8.5 and higher than 3.24°C&2.67°C in
220 SSP2-4.5&RCP4.5. In the lower emission scenarios (SSP1-2.6&RCP2.6) there is a stabilization
221 for the extremes in the second half of 21st century, achieving lowest warming (e.g.,
222 2.23°C&1.92°C for TXx in 2100). This result implies the benefits of mitigation strategies
223 associated with these scenarios (O'Neill et al., 2016). However, the separation for the adjacent
224 pathways (e.g., SSP5-8.5&SSP3-7.0, SSP3-7.0&SSP2-4.5 and SSP2-4.5&SSP1-2.6) usually
225 occurs after 2060s for most indices over Australia. In particular, compared to SSP5-
226 8.5&RCP8.5, if a more aggressive mitigation policy is undertaken (e.g., SSP1-2.6&RCP2.6), it
227 may still take one or two decades to notice its effects on projected changes in temperature
228 extremes over Australia.



229
 230 **Figure 1.** Time series of the anomalies (base period: 1961-1990) for the 14 ETCCDI indices averaged over
 231 Australia (10°S–45°S, 110°E–155°E) from 1950 to 2100, under the historical simulations and Tier 1 experiments of
 232 ScenarioMIP in CMIP6: Hist (grey), SSP1-2.6 (green), SSP2-4.5 (blue), SSP3-7.0 (yellow) and SSP5-8.5 (red) (the
 233 number of models indicated in parentheses in the legend). Solid lines represent the multi-model medians and
 234 shading indicates the full range across the models for each experiment.

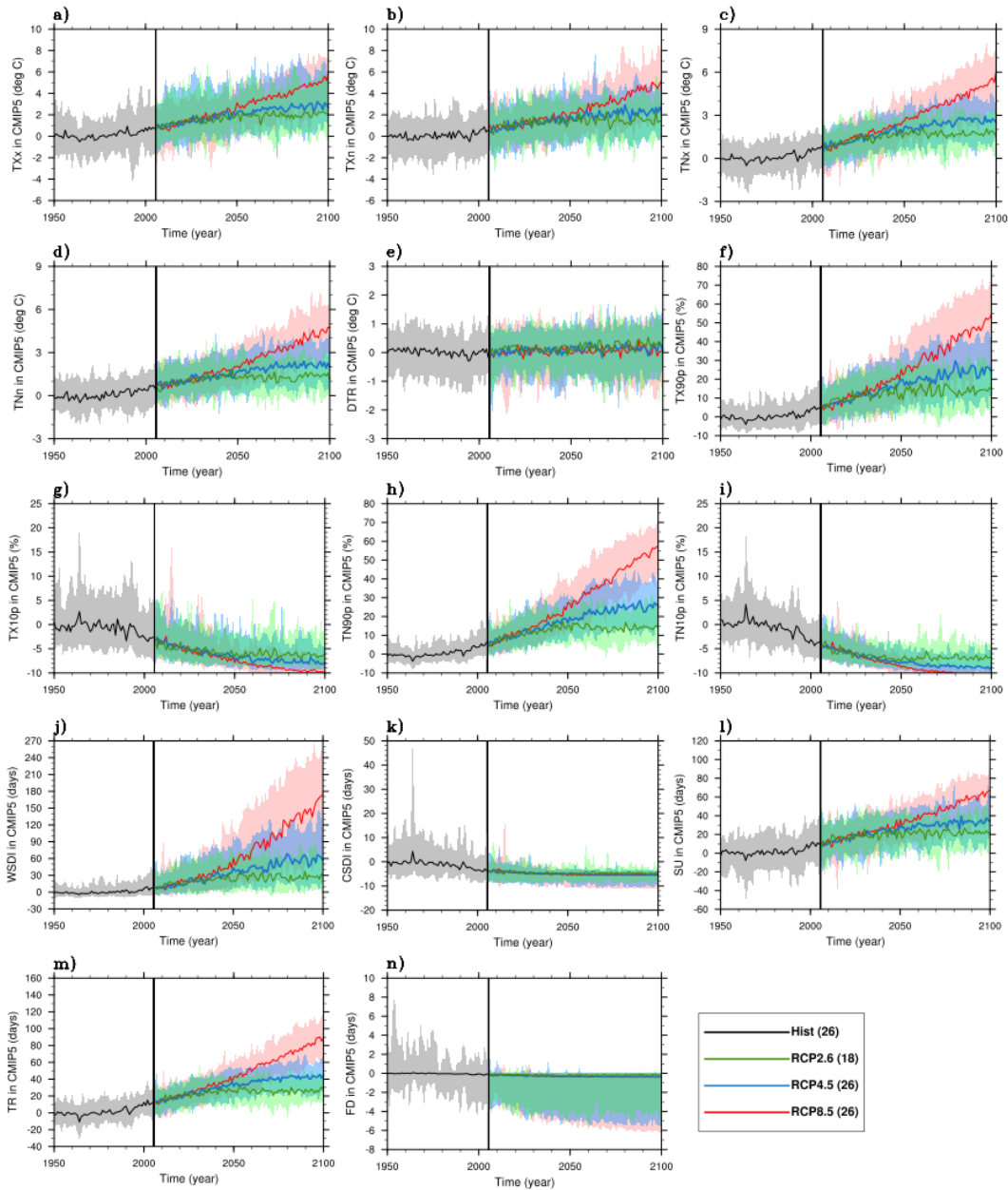
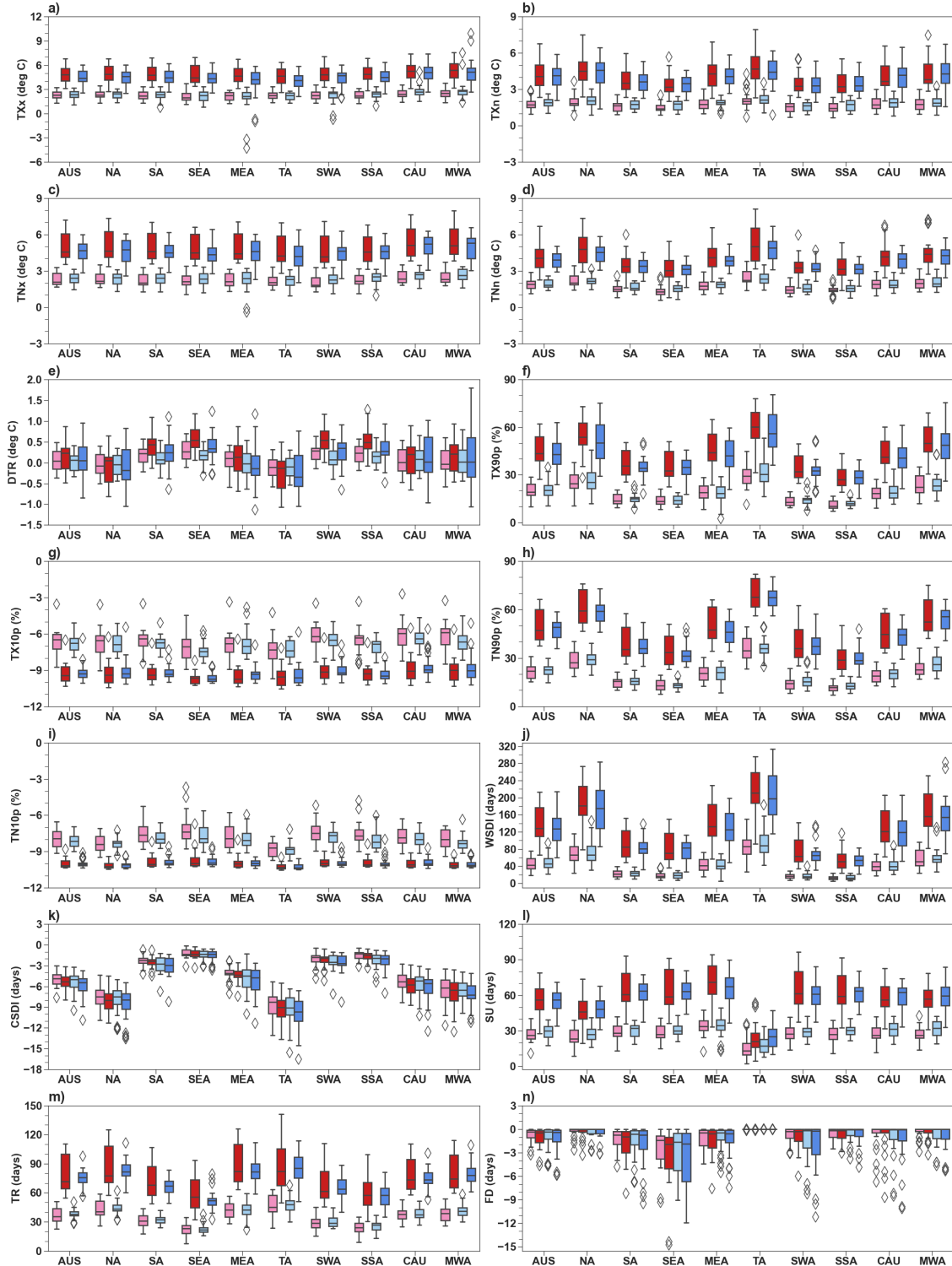


Figure 2. Same as Fig.1, but for CMIP5: Hist (grey), RCP2.6 (green), RCP4.5 (blue), and RCP8.5 (red).

235
236
237

238 To illustrate the spreads and medians of the projected climatological changes in extremes
239 over Australian regions in detail, boxplots for SSP5-8.5&RCP8.5 and SSP1-2.6&RCP2.6 are
240 shown in Figs. 3 and 4, and Figs. S2 and S3 for SSP3-7.0 and SSP2-4.5&RCP4.5. Over the
241 regions, the spreads of the indices in SSPs and RCPs tend to be larger with higher emission
242 pathways and over time, among which some regions such as NA and TA commonly span

243 relatively wider ranges. Compared to RCP8.5, the spreads in SSP5-8.5 are usually larger,
244 especially over the period 2071-2100. As for the multi-model medians, most indices display
245 larger warming trends over TA and lower warming over southern Australian regions (e.g., SSA
246 and SWA); while for other indices (e.g., TXx, TNx and TN10p), there are relatively similar
247 warming levels across the 10 regions. Relative to RCPs, the warming levels for some indices
248 (e.g., TXx, TNn, and WSDI) tends to be higher under the SSPs; in contrast, the relative
249 magnitudes of some indices between RCPs and SSPs, such as TXn and TNx (e.g., Fig. 3b, c and
250 Fig. S3b, c), differ among the regions and the levels of radiative forcing.



251
 252 **Figure 3.** Boxplots of projected changes in the 14 ETCCDI indices over 2071–2100 (bold color) and 2031–2060
 253 (light color) relative to the base period 1961–1990 across 10 Australian regions, under SSP5-8.5 (red) and RCP8.5
 254 (blue). The boxes indicate the interquartile spreads (ranges between the 25th and 75th percentiles), the black lines
 255 within the boxes are the multi-model medians, the whiskers extend to the edges of $1.5 \times$ interquartile ranges and
 256 “outliers” outside of the whiskers are denoted by diamonds.
 257

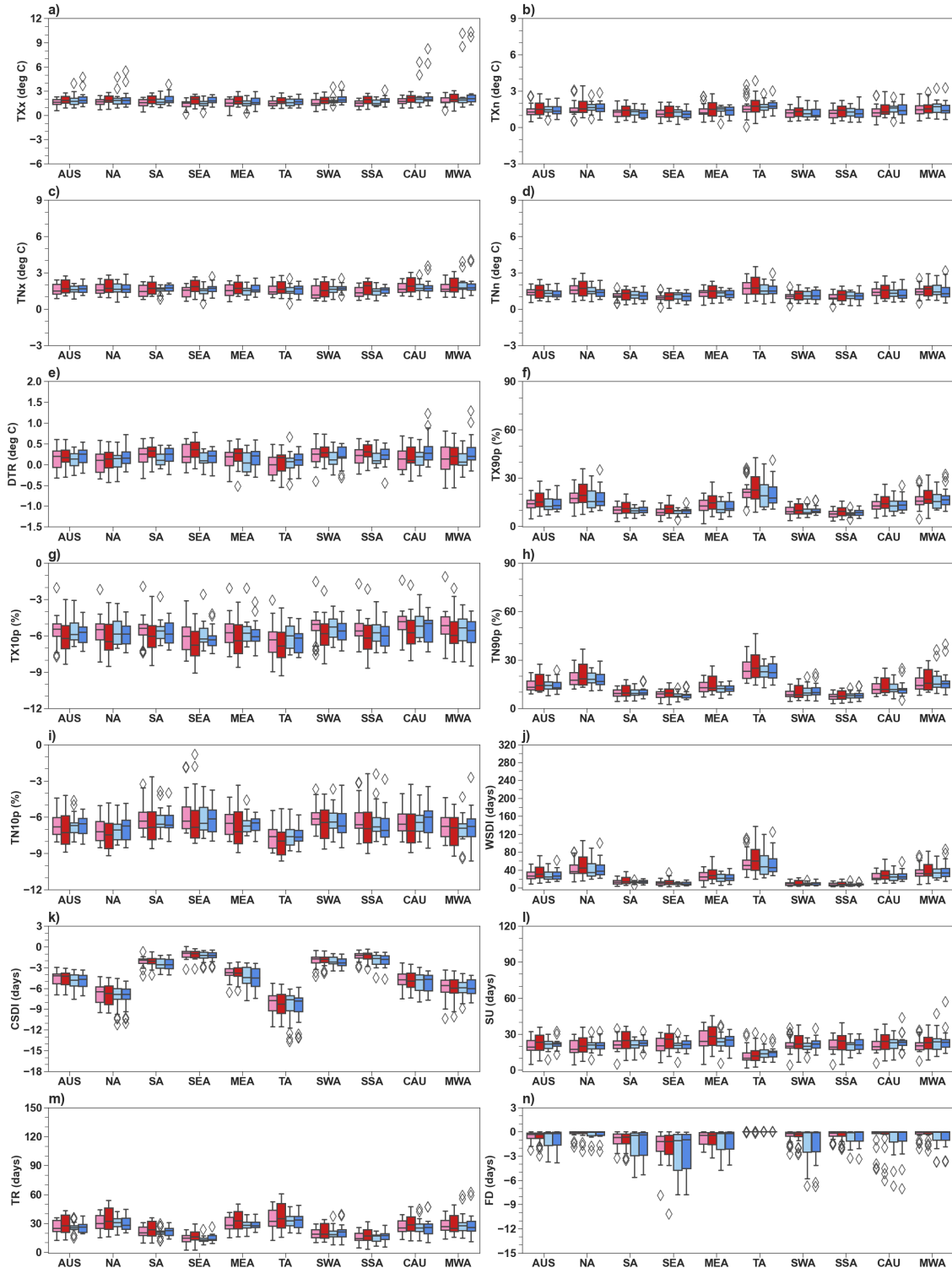


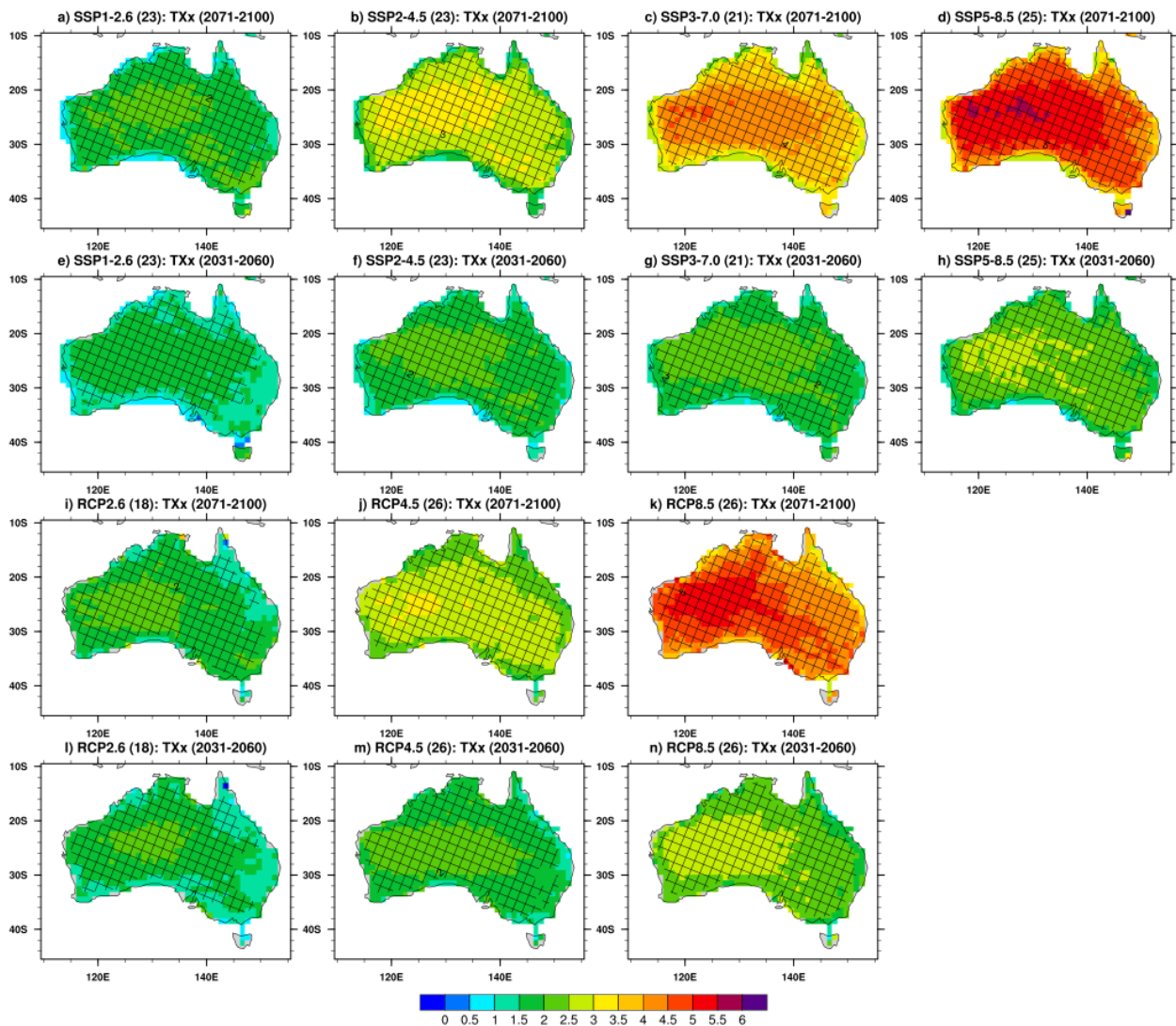
Figure 4. Same as Fig. 3, but for SSP1-2.6 and RCP2.6.

258
259
260

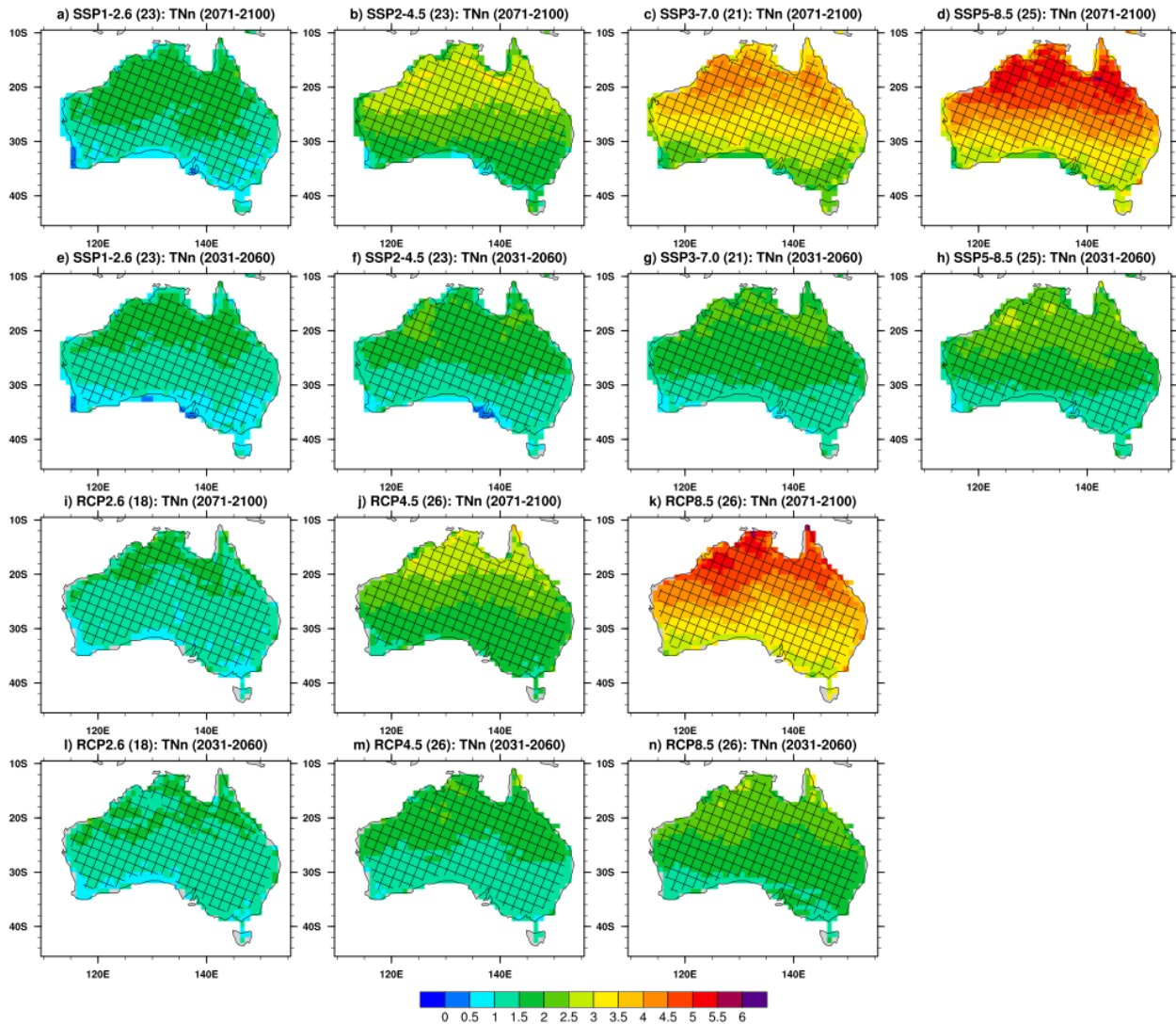
261 Generally, the spatial patterns for the extremes in both CMIP6 and CMIP5 (Figs. 5 and 6;

262 Figs. S4-S15 in the supplementary material) are similar to previous studies (Alexander &

263 Arblaster, 2017). In the highest scenarios for CMIP6 and CMIP5, the extreme indices show a
 264 warmer Australia than other pathways, especially in the end of this century. For most indices
 265 (except DTR in Fig. S6 and FD in Fig. S15), most models (at least 75%) in both CMIP
 266 ensembles project significant changes in extreme temperature indices over most regions of
 267 Australia, both in the middle and the end of the century. However, there are different warming
 268 patterns for some indices. For example, as shown in Fig. 5, the warming pattern in TXx is
 269 relatively consistent among the regions, with the highest warming over central Australia; while
 270 for TNn, Northern Australia displays the most marked warming (Fig. 6).



272 **Figure 5.** Multi-model median changes in TXx for 2071–2100 (a-d; i-k) and 2031–2060 (e-h; l-n) relative to the
 273 base period 1961–2010, under different future scenarios in CMIP6 (SSP1-2.6, SSP2-4.5, SSP3-7.0 and SSP5-8.5)
 274 and CMIP5 (RCP2.6, RCP4.5 and RCP8.5). Hatching indicates that at least 75% of the models for each future
 275 scenario project significant changes at 95% level, based on the two-tailed Student's t-test.
 276



277 **Figure 6.** Same as Fig. 5, but for TNn.
 278
 279

280 Compared to RCP scenarios in CMIP5, the higher projected warming for some extremes
 281 (e.g., TXx and TNn) and the larger spreads in CMIP6 (especially under SSP5-8.5) by the end of
 282 the 21st century is likely related to the different forcings in the SSPs and higher ECS in some
 283 CMIP6 models (e.g., Fyfe et al., 2021; Palmer et al., 2021; Tebaldi et al., 2021). Although there
 284 are similar levels of stratospheric-adjusted radiative forcing in 2100 in RCPs and SSPs, aerosol
 285 emissions, the composition of gases and some radiatively active species (e.g., CO₂ and CH₄) and

286 the resulting ERF in the pathways can be very different (Fyfe et al., 2021; Lurton et al., 2020;
287 Smith et al., 2020; Tebaldi et al., 2021). In addition, the wider inter-model spread of the
288 projected changes under stronger external forcing can result from higher climate sensitivity
289 (Lehner et al., 2020; Tebaldi et al., 2021). As documented in Meehl et al. (2020), 12 of the 39
290 CMIP6 models show higher ECS than the CMIP5 models, some of which can contribute to the
291 wider ranges of projected changes in this study.

292 3.2 Signal-to-Noise Ratio and Time of Emergence

293 The maps of SNR for TXx and TNn in the year 2005 are plotted for BEST, CMIP6 and
294 CMIP5 (Fig. 7), the corresponding signal and noise of which are shown in Figs. S16 and S17,
295 respectively. Although the spatial patterns of noise are relatively similar (Fig. S17), the signals of
296 TXx and TNn show noticeable differences between the observation and the two CMIP
297 ensembles (Fig. S16), which means the resulting SNR in BEST and the two CMIP ensembles
298 differ greatly (Fig. 7). The largest observed SNR for TXx (> 1.2) occurs over central and
299 southwestern regions (Fig. 7a), and for TNn there exhibit negative SNR values (< -0.2) over
300 southwest, northern and southeast parts in Australia (Fig. 7d). In contrast, the SNR of TXx and
301 TNn for both CMIP6 and CMIP5 in 2005 tend to be between 0.2 and 0.8. Although there are
302 differences in the observations and the simulations, the low SNR values in 2005 suggest that the
303 signal for the two temperature extremes over most Australia regions has not emerged from the
304 noise.

305

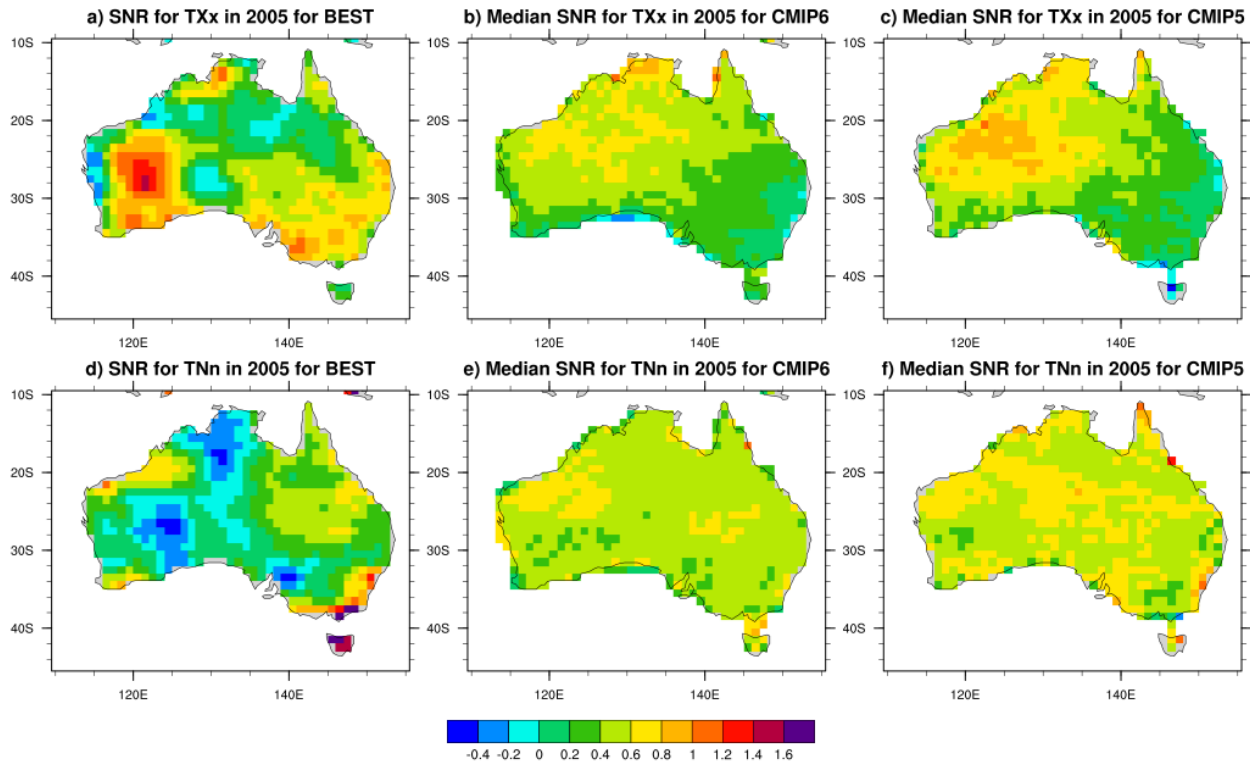
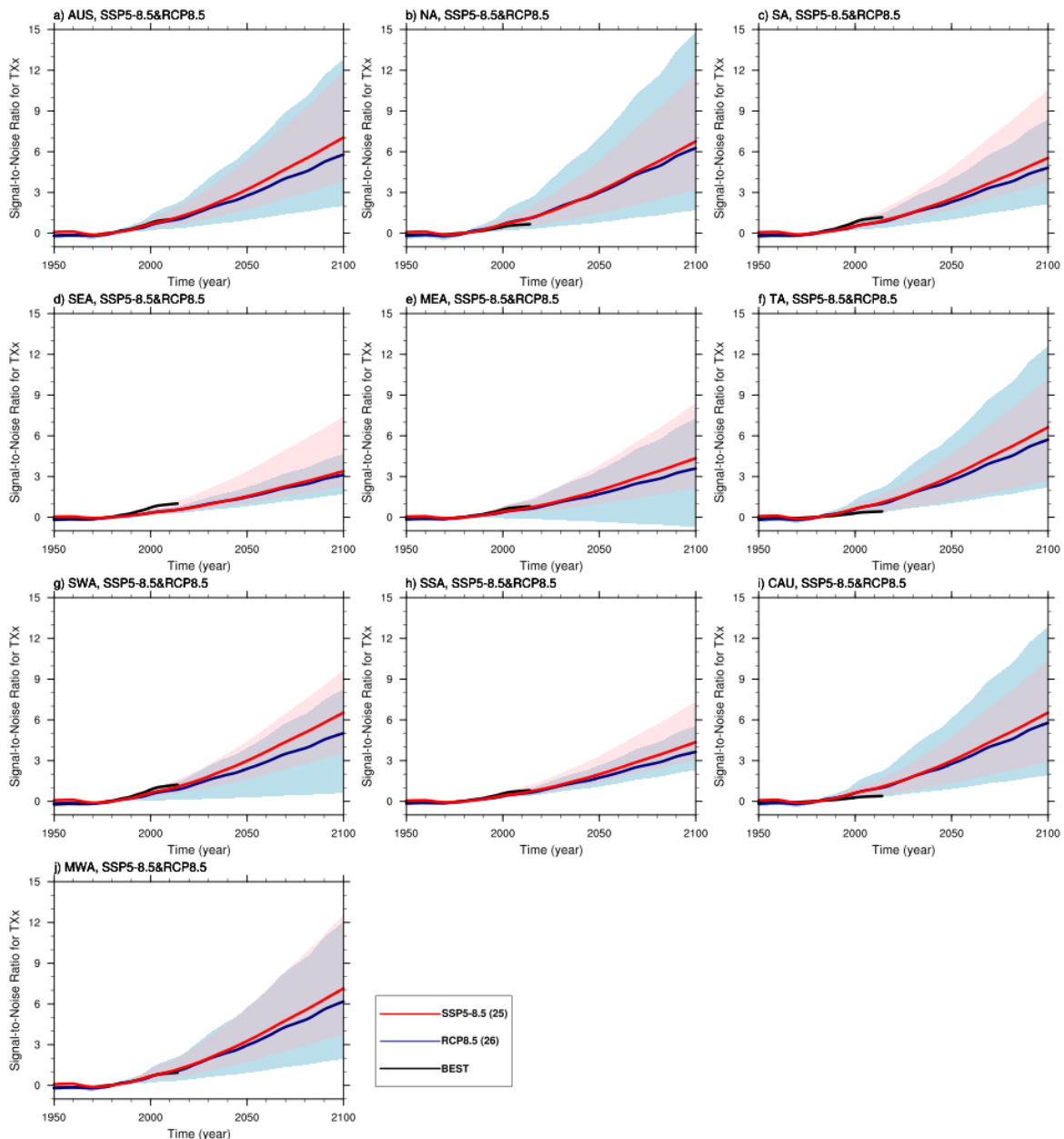


Figure 7. Signal-to-noise ratio (SNR) in the year 2005 for temperature extremes in BEST, CMIP6 and CMIP5. (a) SNR in TXx for BEST; (b) SNR in TXx for the multi-model medians in CMIP6; and (c) SNR in TXx for the multi-model medians in CMIP5. (d-f) Same as (a-c), but for TNn.

As spatial aggregation or averaging may reduce the impact of internal variability (Deser, Knutti, et al., 2012; Hawkins & Sutton, 2009; Lehner et al., 2020), Figs. 8 and 9 show the time series (1950-2100) of SNR for TXx and TNn, which are averaged over each region before the calculation of SNR (the corresponding signal and noise are in the supplementary Figs. S18-S20). For the temporal variations of median SNR over the period 1950-2014, the signal and SNR for TXx in BEST can be within the spread of the two CMIP ensembles over some regions (Fig. 8 and Fig. S18). However, for TNn the signal and SNR are usually outside the ranges of CMIP6 and CMIP5 at the beginning of this century (Fig. 9 and Fig. S19). Despite the influence of observational uncertainty in BEST over Australia (Deng et al., 2021), the above results suggest that the differences between the observed and simulated signal and SNR are mostly related to internal variability (Dai & Bloecker, 2019). In the study by Dai and Bloecker (2019), they

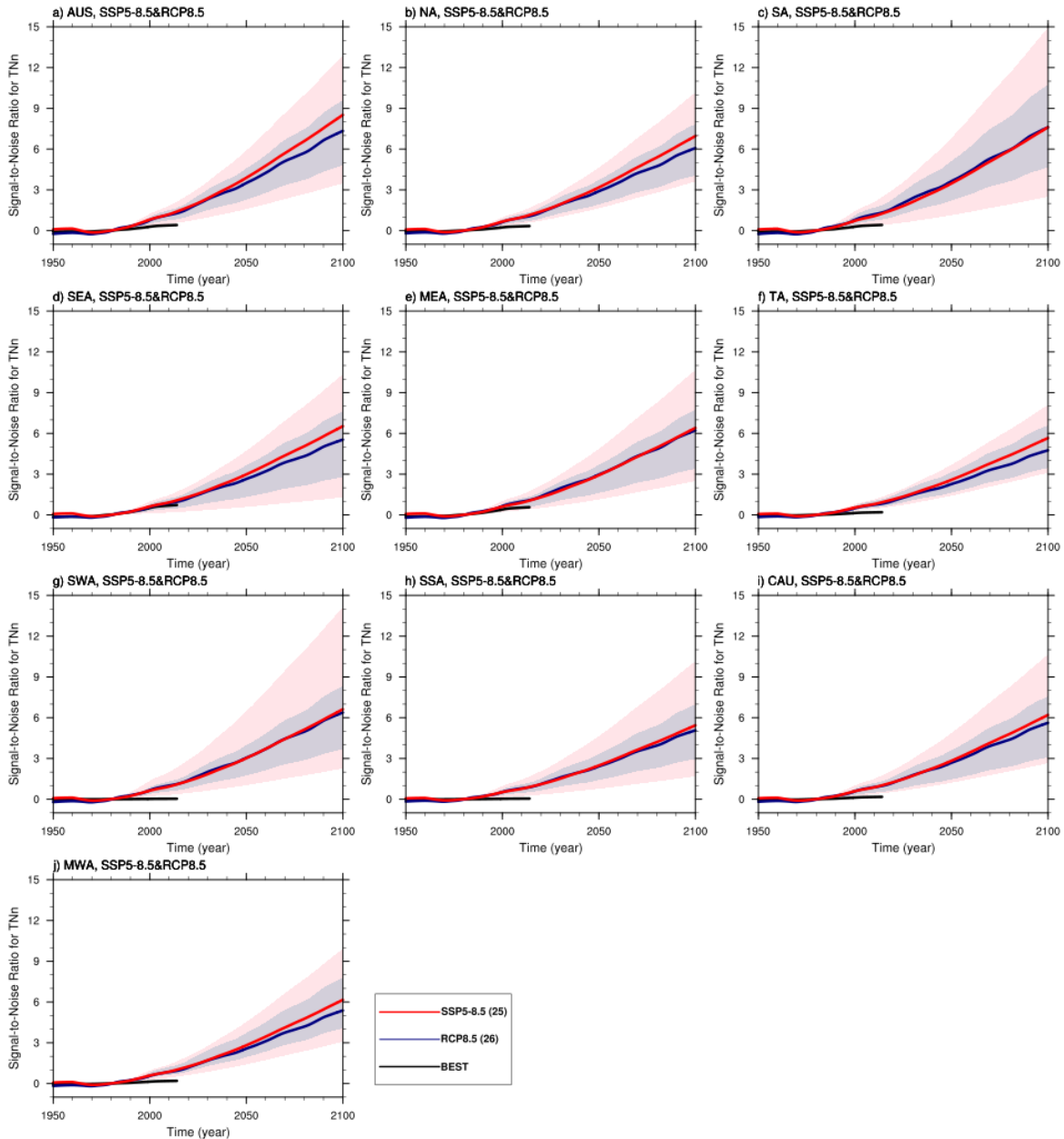
323 concluded that comparing the trends of the observed and modelled precipitation (a variable also
 324 exhibiting relatively large variability), which can represent the signal in some studies (e.g.,
 325 Gaetani et al., 2020), is not appropriate over short timescales and at local and regional scales, as
 326 the observed precipitation changes are still dominated by internal variability.

327



328
 329 **Figure 8.** Time series of signal-to-noise ratio (SNR) in TXx from 1950-2100 over 10 Australian regions for BEST
 330 (black), SSP5-8.5 (red) and RCP8.5 (blue) (the number of models indicated in parentheses in the legend). Solid lines
 331 represent the multi-model medians and shading indicates the full range across the models for each experiment.

332



333
334
335

Figure 9. Same as Fig. 8, but for TNn.

336

Fig. 10 exhibits the spatial distributions of the multi-model median SNR for TXx and

337

TNn under SSP5-8.5 and RCP8.5 in the year 2050, for which the signal is in Figs. S21. Under

338

both SSP5-8.5 and RCP8.5, despite exhibiting different spatial patterns, the magnitudes of SNR

339

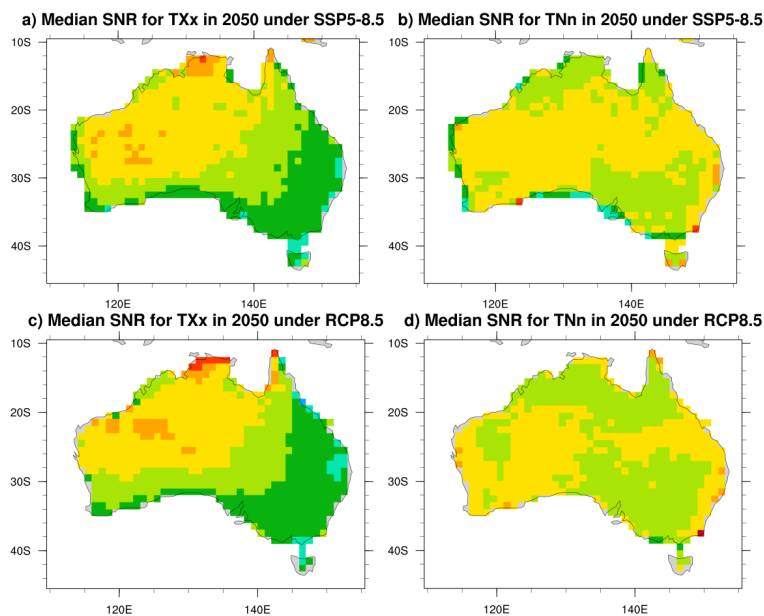
for TXx and TNn are already above 1 over most Australian regions in 2050. For TXx (Fig. 10a,

340

c), there are larger SNR values (>2) over northwest Australia and lower SNR values (>1) over

341 southwest regions. In contrast, the SNR for TNn (Fig. 10b, d) is more than 2 over western and
 342 central Australia and indicates lower values (>1) over tropical and southeast regions. As
 343 described in Frame et al. (2017), around mid-century, the regions exhibiting SNR > 1 suggest
 344 that there would be “unusual” climate compared to the recent climate over 1950-2005; and for
 345 TXx over northwest Australia and TNn over western and central regions, the new climate for the
 346 extremes would be “unfamiliar” (SNR > 2). Compared to RCP8.5, SSP5-8.5 in CMIP6 generally
 347 displays stronger SNR and the corresponding signal for the two indices, which is valid for other
 348 SSPs and RCPs (Figs. S22 and S23).

349



350
 351 **Figure 10.** Median signal-to-noise ratio (SNR) for TXx and TNn under SSP5-8.5 and RCP8.5 in the year 2050. (a)
 352 SNR for TXx under SSP5-8.5 in the year 2050; (b) SNR for TNn under SSP5-8.5 in the year 2050; (c, d) same as (a)
 353 and (b), but for RCP8.5.

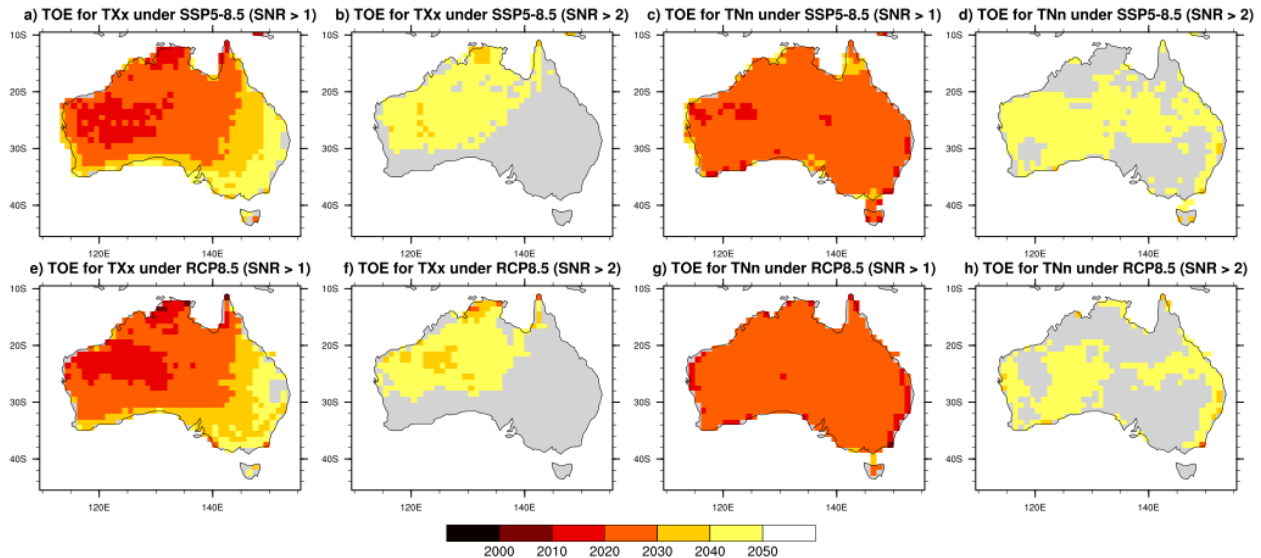
354

355 As for the temporal evolution of SNR (Figs. 8 and 9), in general, the multi-model
 356 medians of SNR in TXx and TNn are slightly larger in SSP5-8.5 than RCP8.5 (e.g., 3.22 under
 357 SSP5-8.5 and 2.77 under RCP8.5 in 2050 over AUS); while over some southern regions for TNn
 358 (e.g., SA, SSA, SWA), the two CMIP ensemble show higher similarity. In addition, the medians

359 of signal and noise for the two indices are also comparable in the two scenarios (Figs. S18-S20).
360 It is noted that the differences in signal between CMIP6 and CMIP5 in the end of the century
361 resemble that shown in Figs. 3a and 3d, which may further imply that the regional climate
362 sensitivity in CMIP6 and CMIP5 is comparable indicated in previous studies (Palmer et al.,
363 2021; Seneviratne & Hauser, 2020). In terms of the inter-model spread, although the spreads of
364 the signals for TXx and TNn in SSP5-8.5 are commonly larger than RCP8.5, in which there are
365 more models showing stronger signal in SSP5-8.5 (Figs. S18 and S19), the ranges in noise (Fig.
366 S20) also contribute to the uncertainty of SNR. Consequently, the relative magnitudes of SNR in
367 SSP5-8.5 and RCP8.5 may change (e.g., Fig. 8a), compared to the signal (e.g., Fig. S18a). For
368 example, the spread of the signal in SSP5-8.5 is slightly larger in the end of the century than
369 RCP8.5; however, influenced by the noise, the resulting range of SNR in SSP5-8.5 becomes
370 narrower. Over the regions, the ranges of SNR for TXx are usually narrower over southern
371 regions (e.g., SSA and SEA); in contrast, for TNn, northern regions such as TA exhibit less
372 uncertainty for SNR and TOE. In other scenarios (Figs. S24-S27), the medians in SNR for TXx
373 and TNn are lower, compared to SSP5-8.5&RCP8.5; and the medians in SSPs are generally still
374 higher than that in RCPs. Also, the spreads of SNR and signal in the lower forcing pathways is
375 generally narrower, consistent with the time series of projected changes.

376 To estimate the TOE for TXx and TNn, we use $SNR > 1$ and $SNR > 2$ as the thresholds
377 (Hawkins and Sutton 2012; Frame et al. 2017; Hawkins et al. 2020) and present the spatial
378 patterns for multi-model median TOE under SSP5-8.5 and RCP8.5 (Fig. 11). As TOE occurring
379 at the end of the century may be a temporary change, which is considered as “pseudo-
380 emergence”, we exclude the TOE occurring after the year 2050 (Abatzoglou et al., 2019;
381 Diffenbaugh & Scherer, 2011; Hawkins et al., 2014; King, Donat, et al., 2015).

382



383

384

385

386

387

Figure 11. Median time of emergence (TOE) for TXx and TNn based on SNR thresholds under SSP5-8.5 and RCP8.5. (a) TOE for TXx under SSP5-8.5 when SNR > 1; (b) TOE for TXx under SSP5-8.5 when SNR > 2; (c, d) same as (a) and (b), but for TNn; (e-h) same as (a-d), but for RCP8.5.

388

389

390

391

392

393

394

395

396

397

398

399

400

Over some central and tropical parts of Australia, the multi-model median TOE in TXx for SNR > 1 can occur as early as the second decade of this century (2010-2020). Generally, the signal emerges earlier over northwestern region than the southeast for both thresholds (Fig. 11a, b, e and f), in which the signal emerges in 2020s for SNR > 1 and 2040s for SNR > 2, as there indicate relative smaller noise and larger signal (Figs. S17 and S21). Over the southeast regions, the TOE occurs within 2030-2050 for SNR > 1. In contrast, for TNn, the signal emerges from the noise in 2020s over Australia (SNR > 1; Fig. 11c and g); while for SNR > 2, the TOE is within the fifth decade (2040-2050) over western and central regions (Fig. 11d and h). Compared to RCP8.5, the multi-model medians of TOE for TXx and TNn in CMIP6 show earlier TOE over more regions based on the threshold SNR > 2, implying the larger median SNR in the middle of this century as shown in Figs. 8 and 9. However, the uncertainty surrounding these TOE estimates remains large (Figs. 8 and 9). For example, for SNR = 2, the range (inter-model spread) of TOE for TXx over AUS can be from 2010s to 2060s (Fig. 8a). For lower scenarios,

401 the multi-model medians of TOE commonly occur later and over smaller regions than the
402 stronger pathways. For example, TOE (SNR > 1) for TNn under SSP2-4.5&RCP4.5 usually can
403 be 10 years later over some southeast regions (Fig. S28g and k) than that shown in SSP5-
404 8.5&RCP4.5 (Fig. 11c and g), as the signal is lower compared to that in higher pathways.

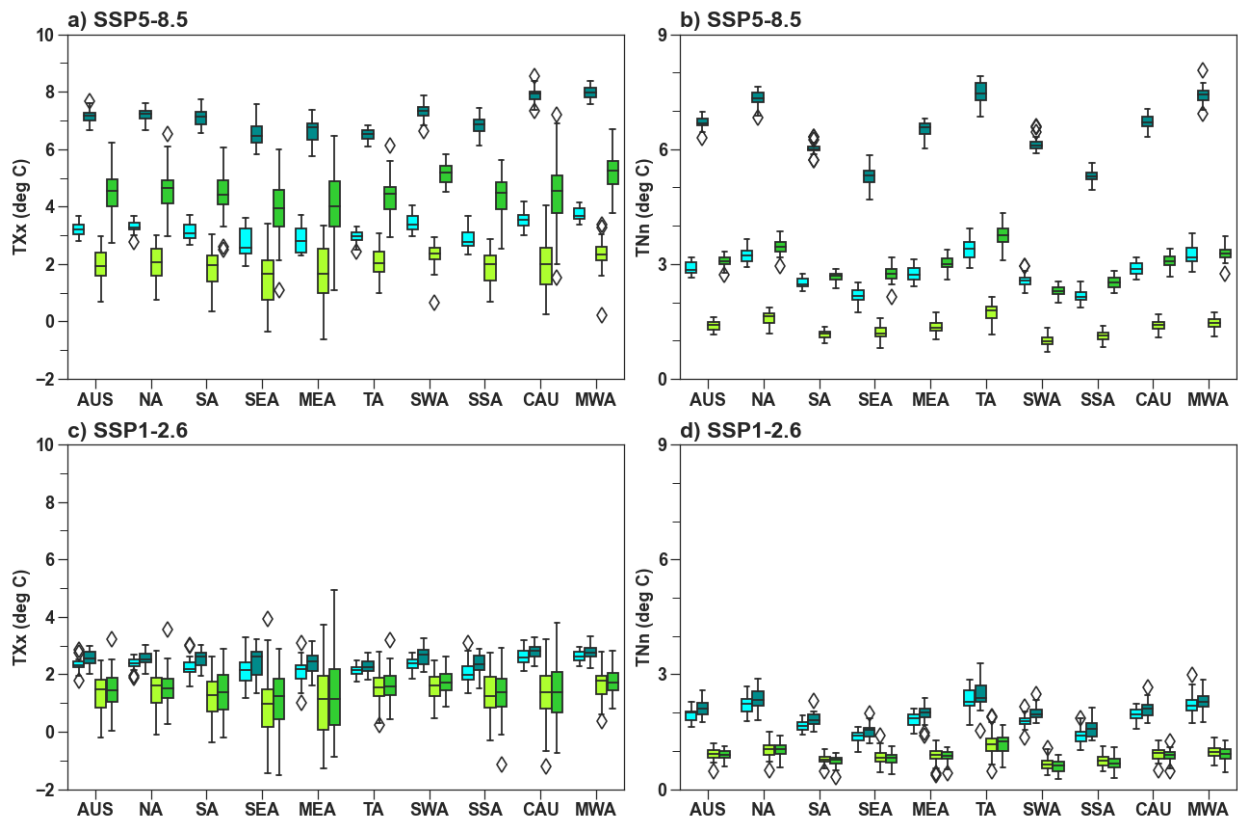
405 The analysis on SNR and TOE has useful implications for Australia. Under the highest-
406 emission scenarios SSP5-8.5&RCP8.5, in which the medians of the signal for TXx are
407 comparable, the early emergence over northwest Australia suggests that there is less time for
408 stakeholders and policy makers to implement effective measures, compared to southeast
409 Australia. In contrast, if under lower scenarios, the TOE for TXx can be postponed, especially
410 for southeast regions which exhibit larger variability for TXx in the extratropics. However, the
411 adaptation policy may change for different extremes, even under same future pathways. For
412 TNn, the TOE (SNR > 1) can occur over most regions even under lower-emission scenarios;
413 while the “unfamiliar” climate (SNR > 2) can be largely postponed if taking a more sustainable
414 pathway (lower emission). It is also noted that the large uncertainty in the estimate of SNR and
415 TOE highlights further challenges for stakeholders and policy makers.

416 3.3 Large Ensembles in CMIP6

417 Previous research has demonstrated the model uncertainty in estimating the effects of
418 internal variability on the TXx and TNn trends, shown in LEs during 1950-2014 over Australian
419 regions (Deng et al., 2021). Therefore, how internal variability influences the projected changes
420 and TOE/SNR (including signal and the noise) needs further investigation. In Fig. 12, which
421 represents the boxplots of projected changes in TXx and TNn for CanESM5-LE and MIROC6-
422 LE over Australian regions under SSP5-8.5 and SSP1-2.6, model uncertainty for representing
423 internal variability still exists, and the relative magnitudes of the spreads for projected changes

424 resemble the results in Figs. 12 and 13 in Deng et al. (2021). The projected changes in TXx for
 425 MIROC6-LE span larger ranges than CanESM5-LE by a factor of ~ 3 or more over the regions,
 426 which can be larger than that in Fig. 3a. Moreover, there exhibit larger ranges of the projected
 427 changes for TXx over SEA, MEA, and SSA, and relatively narrower spreads over TA for
 428 CanESM5-LE and SWA for MIROC6-LE. For TNn, the relative magnitude for the two LEs are
 429 comparable over the regions. The different effects of internal variability for different LEs and
 430 regions complicate the assessment of the uncertainty on projected changes.

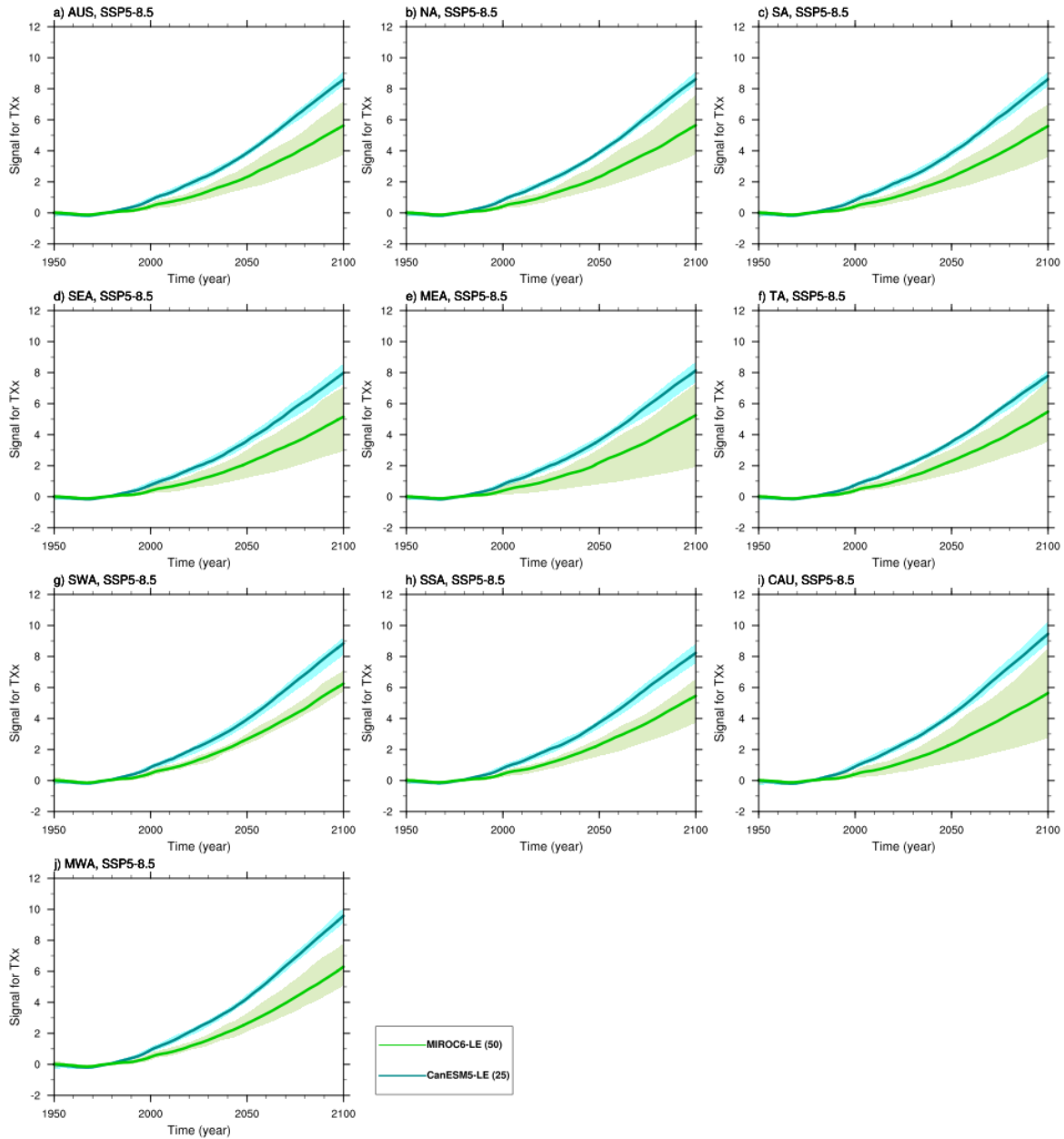
431



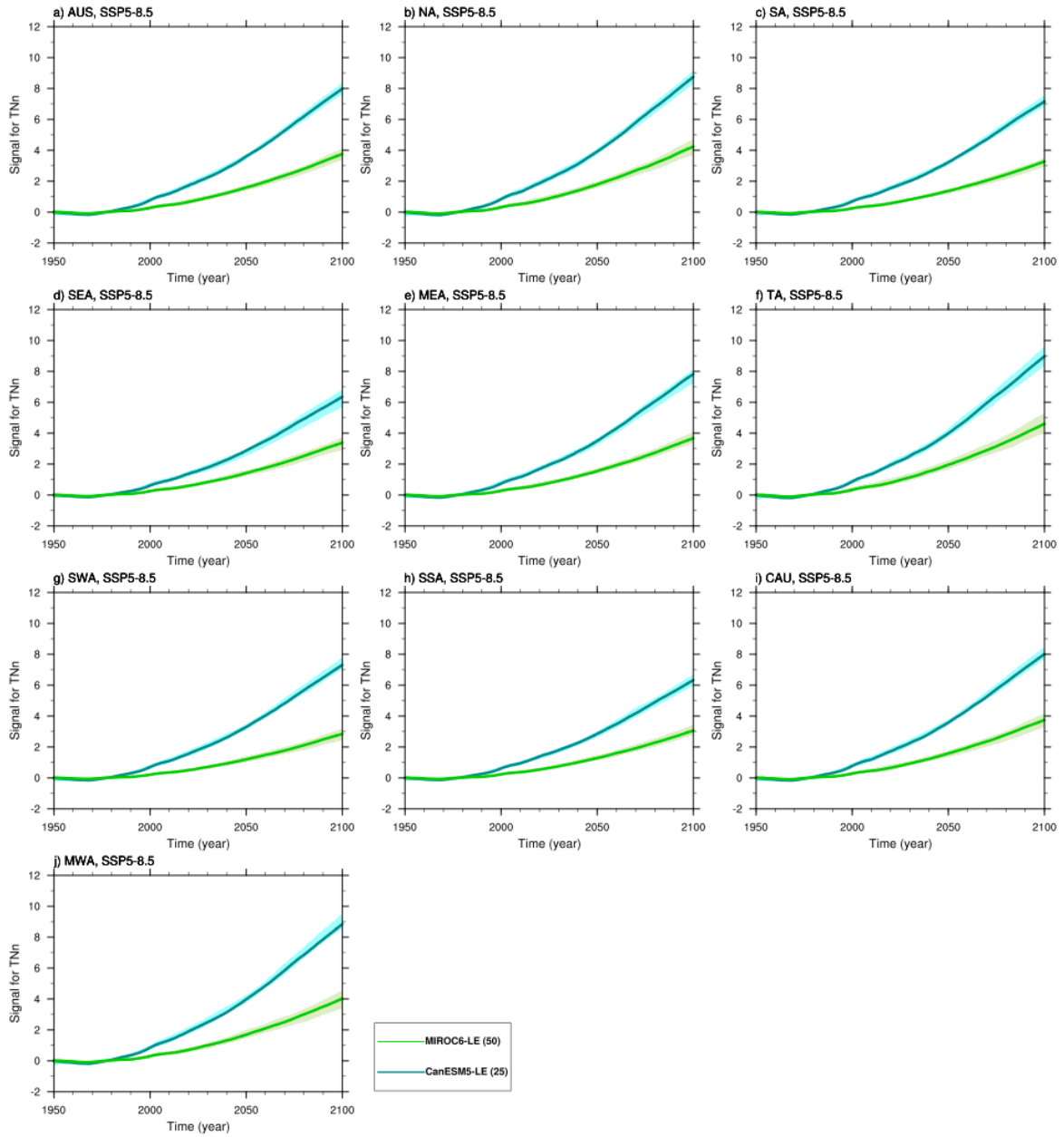
432
 433 **Figure 12.** Boxplots of projected changes in TXx and TNn over 2071–2100 (bold color) and 2031–2060 (light color)
 434 relative to the base period 1961–1990 across 10 Australian regions, for CanESM5-LE (cyan) and MIROC6-LE
 435 (green). (a) TXx under SSP5-8.5; (b) TNn under SSP5-8.5; (c, d) same as (a, b) but for SSP1-2.6. The boxes indicate
 436 the interquartile spreads (ranges between the 25th and 75th percentiles), the black lines within the boxes are the
 437 multi-member medians, the whiskers extend to the edges of $1.5 \times$ interquartile ranges and “outliers” outside of the
 438 whiskers are denoted by diamonds.
 439

440 The temporal evolution of signal and the boxplots of noise for TXx and TNn over
441 Australian regions under SSP5-8.5 are shown in Figs. 13-15, and the resulting SNR in Figs. S29
442 and S30. The relative magnitudes of the ranges in signal and noise over the regions between the
443 two LEs also resemble that for the spread of the TXx and TNn trends shown in Deng et al.
444 (2021). This suggests that internal variability has impacts not only on the uncertainty of signal,
445 but also on the ranges of noise, making the resulting spread of SNR (Figs. S29 and S30) wider or
446 narrower than that for the corresponding signal (Figs. 13 and 14), which introduce further
447 uncertainty in the ranges of TOE. Although the effects of internal variability on TXx and TNn
448 are similar under SSP1-2.6, the temporal evolution of the SNR and the signal for TXx and TNn
449 stabilizes and there are narrower spreads for SNR compared to SSP5-8.5, which is due to the
450 lower magnitude in signal under the lower scenario (Figs. S31-34).

451

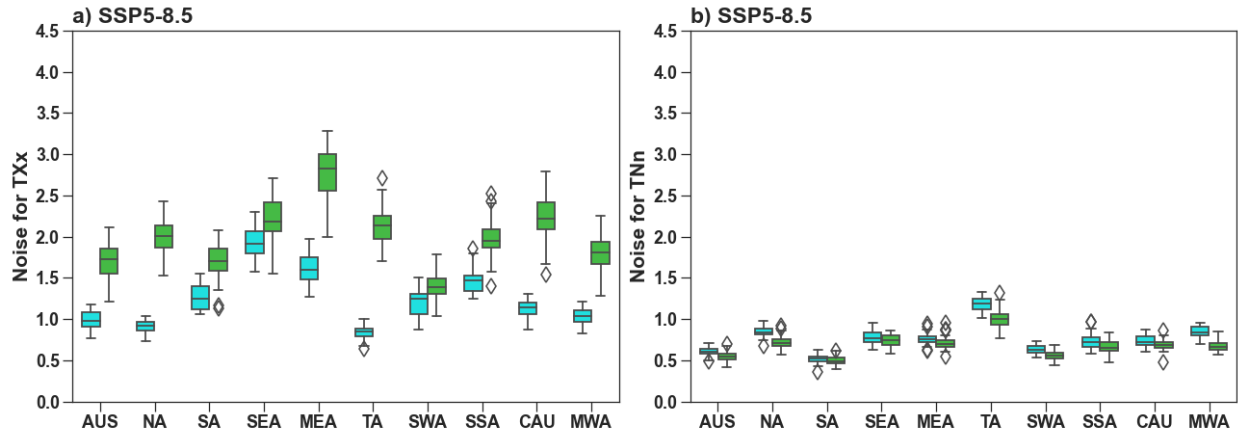


452
 453 **Figure 13.** Time series of signal (unit: K) in TXx from 1950-2100 over 10 Australian regions under SSP5-8.5 for
 454 CanESM5-LE (cyan) and MIROC6-LE (green) (the number of members indicated in parentheses in the legend).
 455 Solid lines represent the multi-member medians and shading indicates the full range across the members for each
 456 LE.
 457



458
459
460

Figure 14. Same as Fig. 13, but for TNn.



461
 462 **Figure 15.** Boxplots of noise (unit: K) in TXx (a) and TNn (b) calculated over the period 1950-2005 across 10
 463 Australian regions, for CanESM5-LE (cyan) and MIROC6-LE (green). The boxes indicate the interquartile spreads
 464 (ranges between the 25th and 75th percentiles), the black lines within the boxes are the multi-member medians, the
 465 whiskers extend to the edges of $1.5 \times$ interquartile ranges and “outliers” outside of the whiskers are denoted by
 466 diamonds.
 467

468 **4 Conclusions**

469 In this study, we analyzed the projected changes for the temperature extremes under
 470 future scenarios (SSP1-2.6, SSP2-4.5, SSP3-7.0 and SSP5-8.5) from the Tier 1 experiment in
 471 ScenarioMIP, which is compared with RCP2.6, RCP4.5 and RCP8.5 in CMIP5. We then use an
 472 SNR framework to estimate the time when the signal of climate change for TXx and TNn
 473 emerges from the internal variability in the two CMIP ensemble. In addition, two LEs in CMIP6
 474 are employed to estimate the effect of internal variability on the projected changes and
 475 TOE/SNR.

476 The projected changes for the multi-model medians of the extremes under the highest
 477 scenario show the strongest warming, and the warming for the indices under SSP3-7.0 fills the
 478 gap between SSP2-4.5 and SSP5-8.5, with SSP1-2.6 showing the least warming, especially in the
 479 end of this century. For some extreme indices (TXx, TXn, TNx, TNn, WSDI and CSDI),
 480 although the spatial patterns of warming can be different, there usually projects “warm-get-
 481 warmer” pattern over Australia. As for the spread in the projections of temperature extremes,

482 they broadly span narrower envelopes for most indices under lower scenarios in the end of this
483 century. If we take a more sustainable pathway (SSP1-2.6), although it may take two or three
484 decades to take effects, the narrower spreads and weaker projected changes pose relatively less
485 challenge for adaptation decisions compared to other scenarios. Compared to other regions, TA
486 usually shows highest warming. However, as the performance of the models over TA usually
487 shows lower scores (Deng et al., 2021), the projected changes for the medians and the spread for
488 the extremes may not be robust (Pierce et al., 2009), which is also applied to other regions such
489 as SSA and SEA.

490 Compared to the counterpart future pathways in CMIP5, the spread in the CMIP6 SSPs
491 are commonly wider than RCPs; and for some extremes (e.g., TXx and TNn), the multi-model
492 medians in SPPs are usually higher as well. This is likely caused by different forcings and higher
493 ECS in some CMIP6 models (e.g., Fyfe et al., 2021; Palmer et al., 2021; Tebaldi et al., 2021).
494 For example, Fyfe et al. (2021) concluded that despite the partly countervailing effect by the
495 background stratospheric aerosols, the higher amount of CO₂ can lead to stronger warming in
496 SSPs. In this study, we also find that for some indices (e.g., TXx), it is the models with higher
497 ECS that usually show warmer evolution than the multi-model medians in SSP5-8.5 (not shown).
498 To further figure out relative importance of each factor, more experiments based on CMIP6
499 models forced by CMIP5 RCP scenarios and/or CMIP5 models forced by CMIP6 SSP scenarios
500 needed be conducted and added to the collection in ScenarioMIP (Fyfe et al., 2021; Tebaldi et
501 al., 2021).

502 We also demonstrate that the medians of SNR for both TXx and TNn in SSPs are
503 commonly higher than in RCPs; and the uncertainty for the SNR of TNn is wider. It is noted that
504 the spreads of SNR for both indices decrease under lower scenarios, which confirms the benefits

505 of lower emission future pathways. Furthermore, the large uncertainty in time of emergence
506 (TOE) result from the inter-model spread of both signal and noise, which is consistent with
507 Hawkins and Sutton (2012). As previous studies concluded that the statistical fit used in the SNR
508 framework can attribute internal variability to the signals (e.g., Hawkins & Sutton, 2012; Kumar
509 & Ganguly, 2018; Lehner et al., 2020), we further illustrate that internal variability can also
510 influence the ranges of noise. To better isolate forced response, dynamical adjustment or LEs can
511 be used (e.g., Lehner et al., 2020; Merrifield et al., 2020). In contrast, using the mean across the
512 range of noise in a LE may be a more appropriate way to represent the expected noise for the
513 model, which needs further investigation.

514 This study suggests that for different extreme temperature indices, the patterns for
515 projected changes and TOE over Australia can be different, which poses large challenge for
516 stakeholders and policymakers. A further effort is to improve the climate models in simulating
517 the physical processes and the internal variability. Unless they are better understood and
518 constrained, the uncertainty of projected changes and TOE will likely continue over future model
519 generations.

520

521 **Conflict of Interest**

522 The authors declare no financial or other conflicts of interests that could have appeared to
523 influence the work reported in this paper.

524

525 **Acknowledgments**

526 We acknowledge two anonymous reviewers for their constructive comments. We thank
527 Edward Hawkins for feedback and comments. This research/project was undertaken with the
528 assistance of resources and services from the National Computational Infrastructure (NCI),
529 which is supported by the Australian Government. We thank the World Climate Research
530 Programme's Working Group on Coupled Modelling, which is responsible for CMIP and
531 coordinated CMIP5 and CMIP6. We further acknowledge the climate modeling groups for
532 producing and making available their model output, the Earth System Grid Federation (ESGF)
533 for archiving the data and providing access, and the multiple funding agencies who support
534 CMIP and ESGF. S.E.P-K. is supported by ARC grant number FT170100106 and CLEX grant
535 number CE170100023.

536

537 **Data Availability Statement**

538 The BEST dataset is obtained from <http://berkeleyearth.org/data>, and the methodological
539 details are provided in the references: Rohde, Muller, Jacobsen, Muller, et al. (2013) and Rohde,
540 Muller, Jacobsen, Perlmutter, et al. (2013). The CMIP6 and CMIP5 outputs can be downloaded
541 from the Earth System Grid Federation (<https://esgf-node.llnl.gov/search/cmip6/> and [https://esgf-](https://esgf-node.llnl.gov/search/cmip5/)
542 [node.llnl.gov/search/cmip5/](https://esgf-node.llnl.gov/search/cmip5/)). Code for the temperature extremes in the ETCCDI indices is
543 archived at <https://doi.org/10.5281/zenodo.4903200> (Deng, 2021).

544

545 **References**

546 Abatzoglou, J. T., Williams, A. P., & Barbero, R. (2019). Global emergence of anthropogenic climate change in fire
547 weather indices. *Geophysical Research Letters*, 46(1), 326-336. <https://doi.org/10.1029/2018gl080959>

- 548 Alexander, L. V., & Arblaster, J. M. (2017). Historical and projected trends in temperature and precipitation
549 extremes in Australia in observations and CMIP5. *Weather and Climate Extremes*, 15, 34-56.
550 <https://doi.org/10.1016/j.wace.2017.02.001>
- 551 Barnes, E. A., Hurrell, J. W., Ebert-Uphoff, I., Anderson, C., & Anderson, D. (2019). Viewing forced climate
552 patterns through an AI Lens. *Geophysical Research Letters*, 46(22), 13389-13398.
553 <https://doi.org/10.1029/2019gl084944>
- 554 Barsugli, J. J., & Battisti, D. S. (1998). The basic effects of atmosphere-ocean thermal coupling on midlatitude
555 variability. *Journal of the Atmospheric Sciences*, 55(4), 477-493. [https://doi.org/10.1175/1520-0469\(1998\)055<0477:Tbeoao>2.0.Co;2](https://doi.org/10.1175/1520-0469(1998)055<0477:Tbeoao>2.0.Co;2)
- 557 Batibeniz, F., Ashfaq, M., Diffenbaugh, N. S., Key, K., Evans, K. J., Turuncoglu, U. U., et al. (2020). Doubling of
558 U.S. population exposure to climate extremes by 2050. *Earth's Future*, 8(4), e2019EF001421.
559 <https://doi.org/10.1029/2019ef001421>
- 560 Beaumont, L. J., Pitman, A., Perkins, S., Zimmermann, N. E., Yoccoz, N. G., & Thuiller, W. (2011). Impacts of
561 climate change on the world's most exceptional ecoregions. *Proceedings of the National Academy of
562 Sciences of the United States of America*, 108(6), 2306-2311. <https://doi.org/10.1073/pnas.1007217108>
- 563 Bell, B., Hersbach, H., Simmons, A., Berrisford, P., Dahlgren, P., Horányi, A., et al. (2021). The ERA5 global
564 reanalysis: Preliminary extension to 1950. *Quarterly Journal of the Royal Meteorological Society*,
565 147(741), 4186-4227. <https://doi.org/10.1002/qj.4174>
- 566 Cleveland, W. S. (1979). Robust locally weighted regression and smoothing scatterplots. *Journal of the American
567 Statistical Association*, 74(368), 829-836. <https://doi.org/10.2307/2286407>
- 568 Compo, G. P., Whitaker, J. S., Sardeshmukh, P. D., Matsui, N., Allan, R. J., Yin, X., et al. (2011). The twentieth
569 century reanalysis project. *Quarterly Journal of the Royal Meteorological Society*, 137(654), 1-28.
570 <https://doi.org/10.1002/qj.776>
- 571 Dai, A., & Bloecker, C. E. (2019). Impacts of internal variability on temperature and precipitation trends in large
572 ensemble simulations by two climate models. *Climate Dynamics*, 52(1-2), 289-306.
573 <https://doi.org/10.1007/s00382-018-4132-4>
- 574 Deng, X. (2021). Code for temperature extremes in ETCCDI indices based on the NCAR Command Language.
575 *Zenodo*. <https://doi.org/10.5281/zenodo.4903200>
- 576 Deng, X., Perkins-Kirkpatrick, S. E., Lewis, S. C., & Ritchie, E. A. (2021). Evaluation of extreme temperatures over
577 Australia in the historical simulations of CMIP5 and CMIP6 models. *Earth's Future*, 9(7), e2020EF001902.
578 <https://doi.org/10.1029/2020ef001902>
- 579 Deser, C. (2020). "Certain uncertainty: The role of internal climate variability in projections of regional climate
580 change and risk management". *Earth's Future*, 8(12), e2020EF001854.
581 <https://doi.org/10.1029/2020ef001854>
- 582 Deser, C., Knutti, R., Solomon, S., & Phillips, A. S. (2012). Communication of the role of natural variability in
583 future North American climate. *Nature Climate Change*, 2(11), 775-779.
584 <https://doi.org/10.1038/nclimate1562>
- 585 Deser, C., Lehner, F., Rodgers, K. B., Ault, T., Delworth, T. L., DiNezio, P. N., et al. (2020). Insights from Earth
586 system model initial-condition large ensembles and future prospects. *Nature Climate Change*, 10(4), 277-
587 286. <https://doi.org/10.1038/s41558-020-0731-2>
- 588 Deser, C., Phillips, A., Bourdette, V., & Teng, H. Y. (2012). Uncertainty in climate change projections: the role of
589 internal variability. *Climate Dynamics*, 38(3-4), 527-546. <https://doi.org/10.1007/s00382-010-0977-x>
- 590 Deutsch, C. A., Tewksbury, J. J., Huey, R. B., Sheldon, K. S., Ghalambor, C. K., Haak, D. C., et al. (2008). Impacts
591 of climate warming on terrestrial ectotherms across latitude. *Proceedings of the National Academy of
592 Sciences of the United States of America*, 105(18), 6668-6672. <https://doi.org/10.1073/pnas.0709472105>
- 593 Diffenbaugh, N. S., & Scherer, M. (2011). Observational and model evidence of global emergence of permanent,
594 unprecedented heat in the 20th and 21st centuries. *Climatic Change*, 107(3-4), 615-624.
595 <https://doi.org/10.1007/s10584-011-0112-y>
- 596 Eyring, V., Bony, S., Meehl, G. A., Senior, C. A., Stevens, B., Stouffer, R. J., et al. (2016). Overview of the Coupled
597 Model Intercomparison Project Phase 6 (CMIP6) experimental design and organization. *Geoscientific
598 Model Development*, 9(5), 1937-1958. <https://doi.org/10.5194/gmd-9-1937-2016>
- 599 Fischer, E. M., Sedláček, J., Hawkins, E., & Knutti, R. (2014). Models agree on forced response pattern of
600 precipitation and temperature extremes. *Geophysical Research Letters*, 41(23), 8554-8562.
601 <https://doi.org/10.1002/2014gl062018>
- 602 Frame, D., Joshi, M., Hawkins, E., Harrington, L. J., & de Roiste, M. (2017). Population-based emergence of
603 unfamiliar climates. *Nature Climate Change*, 7(6), 407-411. <https://doi.org/10.1038/nclimate3297>

- 604 Fyfe, J. C., Kharin, V. V., Santer, B. D., Cole, J. N. S., & Gillett, N. P. (2021). Significant impact of forcing
605 uncertainty in a large ensemble of climate model simulations. *Proceedings of the National Academy of*
606 *Sciences of the United States of America*, 118(23), e2016549118. <https://doi.org/10.1073/pnas.2016549118>
- 607 Gaetani, M., Janicot, S., Vrac, M., Famien, A. M., & Sultan, B. (2020). Robust assessment of the time of emergence
608 of precipitation change in West Africa. *Scientific Reports*, 10(1), 7670. <https://doi.org/10.1038/s41598-020-63782-2>
- 609
- 610 Giorgi, F., & Bi, X. (2009). Time of emergence (TOE) of GHG-forced precipitation change hot-spots. *Geophysical*
611 *Research Letters*, 36(6), L06709. <https://doi.org/10.1029/2009gl037593>
- 612 Grose, M. R., Narsey, S., Delage, F. P., Dowdy, A. J., Bador, M., Boschat, G., et al. (2020). Insights From CMIP6
613 for Australia's Future Climate. *Earth's Future*, 8(5), e2019EF001469.
614 <https://doi.org/10.1029/2019ef001469>
- 615 Hawkins, E., Anderson, B., Diffenbaugh, N., Mahlstein, I., Betts, R., Hegerl, G., et al. (2014). Uncertainties in the
616 timing of unprecedented climates. *Nature*, 511(7507), E3-E5. <https://doi.org/10.1038/nature13523>
- 617 Hawkins, E., Frame, D., Harrington, L., Joshi, M., King, A., Rojas, M., et al. (2020). Observed emergence of the
618 climate change signal: From the familiar to the unknown. *Geophysical Research Letters*, 47(6),
619 e2019GL086259. <https://doi.org/10.1029/2019gl086259>
- 620 Hawkins, E., & Sutton, R. (2009). The potential to narrow uncertainty in regional climate predictions. *Bulletin of the*
621 *American Meteorological Society*, 90(8), 1095-1108. <https://doi.org/10.1175/2009bams2607.1>
- 622 Hawkins, E., & Sutton, R. (2012). Time of emergence of climate signals. *Geophysical Research Letters*, 39(1),
623 L01702. <https://doi.org/10.1029/2011gl050087>
- 624 Hersbach, H., Bell, B., Berrisford, P., Hirahara, S., Horányi, A., Muñoz-Sabater, J., et al. (2020). The ERA5 global
625 reanalysis. *Quarterly Journal of the Royal Meteorological Society*, 146(730), 1999-2049.
626 <https://doi.org/10.1002/qj.3803>
- 627 Intergovernmental Panel on Climate Change. (2021). *Climate Change 2021: The physical science basis.*
628 *Contribution of Working Group I to the sixth assessment report of the Intergovernmental Panel on Climate*
629 *Change* (V. Masson-Delmotte, P. Zhai, A. Pirani, S. L. Connors, C. Péan, S. Berger, N. Caud, Y. Chen, L.
630 Goldfarb, M. I. Gomis, M. Huang, K. Leitzell, E. Lonnoy, J. B. R. Matthews, T. K. Maycock, T.
631 Waterfield, O. Yelekçi, R. Yu, & B. Zhou Eds.). Cambridge, UK and New York, NY, USA: Cambridge
632 University Press.
- 633 Jones, D. A., Wang, W., & Fawcett, R. (2009). High-quality spatial climate data-sets for Australia. *Australian*
634 *Meteorological and Oceanographic Journal*, 58(4), 233-248. <https://doi.org/10.22499/2.5804.003>
- 635 Kalnay, E., Kanamitsu, M., Kistler, R., Collins, W., Deaven, D., Gandin, L., et al. (1996). The NCEP/NCAR 40-
636 year reanalysis project. *Bulletin of the American Meteorological Society*, 77(3), 437-472.
637 [https://doi.org/10.1175/1520-0477\(1996\)077<0437:Tnyrp>2.0.Co;2](https://doi.org/10.1175/1520-0477(1996)077<0437:Tnyrp>2.0.Co;2)
- 638 Kanamitsu, M., Ebisuzaki, W., Woollen, J., Yang, S. K., Hnilo, J. J., Fiorino, M., et al. (2002). NCEP-DOE AMIP-
639 II Reanalysis (R-2). *Bulletin of the American Meteorological Society*, 83(11), 1631-1643.
640 [https://doi.org/10.1175/bams-83-11-1631\(2002\)083<1631:Nar>2.3.Co;2](https://doi.org/10.1175/bams-83-11-1631(2002)083<1631:Nar>2.3.Co;2)
- 641 King, A. D., Donat, M. G., Fischer, E. M., Hawkins, E., Alexander, L. V., Karoly, D. J., et al. (2015). The timing of
642 anthropogenic emergence in simulated climate extremes. *Environmental Research Letters*, 10(9), 094015.
643 <https://doi.org/10.1088/1748-9326/10/9/094015>
- 644 King, A. D., van Oldenborgh, G. J., Karoly, D. J., Lewis, S. C., & Cullen, H. (2015). Attribution of the record high
645 Central England temperature of 2014 to anthropogenic influences. *Environmental Research Letters*, 10(5).
646 <https://doi.org/10.1088/1748-9326/10/5/054002>
- 647 Kumar, D., & Ganguly, A. R. (2018). Intercomparison of model response and internal variability across climate
648 model ensembles. *Climate Dynamics*, 51(1-2), 207-219. <https://doi.org/10.1007/s00382-017-3914-4>
- 649 Lehner, F., Deser, C., Maher, N., Marotzke, J., Fischer, E. M., Brunner, L., et al. (2020). Partitioning climate
650 projection uncertainty with multiple large ensembles and CMIP5/6. *Earth System Dynamics*, 11(2), 491-
651 508. <https://doi.org/10.5194/esd-11-491-2020>
- 652 Lurton, T., Balkanski, Y., Bastrikov, V., Bekki, S., Bopp, L., Braconnot, P., et al. (2020). Implementation of the
653 CMIP6 forcing data in the IPSL-CM6A-LR model. *Journal of Advances in Modeling Earth Systems*, 12(4),
654 e2019MS001940. <https://doi.org/10.1029/2019ms001940>
- 655 Mahlstein, I., Hegerl, G., & Solomon, S. (2012). Emerging local warming signals in observational data. *Geophysical*
656 *Research Letters*, 39(21), L21711. <https://doi.org/10.1029/2012gl053952>
- 657 Mahlstein, I., Knutti, R., Solomon, S., & Portmann, R. W. (2011). Early onset of significant local warming in low
658 latitude countries. *Environmental Research Letters*, 6(3), 034009. <https://doi.org/10.1088/1748-9326/6/3/034009>
- 659

- 660 Mankin, J. S., Lehner, F., Coats, S., & McKinnon, K. A. (2020). The value of initial condition large ensembles to
 661 robust adaptation decision-making. *Earth's Future*, 8(10), e2012EF001610.
 662 <https://doi.org/10.1029/2020ef001610>
- 663 Meehl, G. A., Senior, C. A., Eyring, V., Flato, G., Lamarque, J. F., Stouffer, R. J., et al. (2020). Context for
 664 interpreting equilibrium climate sensitivity and transient climate response from the CMIP6 Earth system
 665 models. *Science Advances*, 6(26), eaba1981. <https://doi.org/10.1126/sciadv.aba1981>
- 666 Merrifield, A. L., Brunner, L., Lorenz, R., Medhaug, I., & Knutti, R. (2020). An investigation of weighting schemes
 667 suitable for incorporating large ensembles into multi-model ensembles. *Earth System Dynamics*, 11(3),
 668 807-834. <https://doi.org/10.5194/esd-11-807-2020>
- 669 O'Neill, B. C., Tebaldi, C., van Vuuren, D. P., Eyring, V., Friedlingstein, P., Hurtt, G., et al. (2016). The Scenario
 670 Model Intercomparison Project (ScenarioMIP) for CMIP6. *Geoscientific Model Development*, 9(9), 3461-
 671 3482. <https://doi.org/10.5194/gmd-9-3461-2016>
- 672 Ossó, A., Allan, R. P., Hawkins, E., Shaffrey, L., & Maraun, D. (2021). Emerging new climate extremes over
 673 Europe. *Climate Dynamics*. <https://doi.org/10.1007/s00382-021-05917-3>
- 674 Palmer, T. E., Booth, B. B. B., & McSweeney, C. F. (2021). How does the CMIP6 ensemble change the picture for
 675 European climate projections? *Environmental Research Letters*, 16(9), 094042.
 676 <https://doi.org/10.1088/1748-9326/ac1ed9>
- 677 Perkins, S. E., Moise, A., Whetton, P., & Katzfey, J. (2014). Regional changes of climate extremes over Australia –
 678 A comparison of regional dynamical downscaling and global climate model simulations. *International
 679 journal of climatology*, 34(12), 3456-3478. <https://doi.org/10.1002/joc.3927>
- 680 Perkins-Kirkpatrick, S. E., Fischer, E. M., Angélil, O., & Gibson, P. B. (2017). The influence of internal climate
 681 variability on heatwave frequency trends. *Environmental Research Letters*, 12(4).
 682 <https://doi.org/10.1088/1748-9326/aa63fe>
- 683 Pierce, D. W., Barnett, T. P., Santer, B. D., & Gleckler, P. J. (2009). Selecting global climate models for regional
 684 climate change studies. *Proceedings of the National Academy of Sciences of the United States of America*,
 685 106(21), 8441-8446. <https://doi.org/10.1073/pnas.0900094106>
- 686 Riahi, K., van Vuuren, D. P., Kriegler, E., Edmonds, J., O'Neill, B. C., Fujimori, S., et al. (2017). The Shared
 687 Socioeconomic Pathways and their energy, land use, and greenhouse gas emissions implications: An
 688 overview. *Global Environmental Change*, 42, 153-168. <https://doi.org/10.1016/j.gloenvcha.2016.05.009>
- 689 Rohde, R., Muller, R., Jacobsen, R., Muller, E., Perlmutter, S., Rosenfeld, A., et al. (2013). A new estimate of the
 690 average Earth surface land temperature spanning 1753 to 2011. *Geoinformatics and Geostatistics: An
 691 Overview*, 1(1). <https://doi.org/10.4172/2327-4581.1000101>
- 692 Rohde, R., Muller, R., Jacobsen, R., Perlmutter, S., Rosenfeld, A., Wurtele, J., et al. (2013). Berkeley Earth
 693 temperature averaging process. *Geoinformatics and Geostatistics: An Overview*, 1(2).
 694 <https://doi.org/10.4172/2327-4581.1000103>
- 695 Santer, B. D., Mears, C., Doutriaux, C., Caldwell, P., Gleckler, P. J., Wigley, T. M. L., et al. (2011). Separating
 696 signal and noise in atmospheric temperature changes: The importance of timescale. *Journal of Geophysical
 697 Research: Atmospheres*, 116(D22), D22105. <https://doi.org/10.1029/2011jd016263>
- 698 Seneviratne, S. I., & Hauser, M. (2020). Regional climate sensitivity of climate extremes in CMIP6 versus CMIP5
 699 multi-model ensembles. *Earth's Future*, 8(9), e2019EF001474. <https://doi.org/10.1029/2019EF001474>
- 700 Sillmann, J., Kharin, V. V., Zhang, X., Zwiers, F. W., & Bronaugh, D. (2013). Climate extremes indices in the
 701 CMIP5 multimodel ensemble: Part 1. Model evaluation in the present climate. *Journal of Geophysical
 702 Research: Atmospheres*, 118(4), 1716-1733. <https://doi.org/10.1002/jgrd.50203>
- 703 Sillmann, J., Kharin, V. V., Zwiers, F. W., Zhang, X., & Bronaugh, D. (2013). Climate extremes indices in the
 704 CMIP5 multimodel ensemble: Part 2. Future climate projections. *Journal of Geophysical Research:
 705 Atmospheres*, 118(6), 2473-2493. <https://doi.org/10.1002/jgrd.50188>
- 706 Smith, C. J., Kramer, R. J., Myhre, G., Alterskjær, K., Collins, W., Sima, A., et al. (2020). Effective radiative
 707 forcing and adjustments in CMIP6 models. *Atmospheric Chemistry and Physics*, 20(16), 9591-9618.
 708 <https://doi.org/10.5194/acp-20-9591-2020>
- 709 Sutton, R., Suckling, E., & Hawkins, E. (2015). What does global mean temperature tell us about local climate?
 710 *Philosophical Transactions of the Royal Society A: Mathematical, Physical and Engineering Sciences*,
 711 373(2054), 20140426. <https://doi.org/10.1098/rsta.2014.0426>
- 712 Tan, X., Gan, T. Y., & Horton, D. E. (2018). Projected timing of perceivable changes in climate extremes for
 713 terrestrial and marine ecosystems. *Global Change Biology*, 24(10), 4696-4708.
 714 <https://doi.org/10.1111/gcb.14329>

- 715 Tebaldi, C., Debeire, K., Eyring, V., Fischer, E., Fyfe, J., Friedlingstein, P., et al. (2021). Climate model projections
716 from the Scenario Model Intercomparison Project (ScenarioMIP) of CMIP6. *Earth System Dynamics*,
717 *12*(1), 253-293. <https://doi.org/10.5194/esd-12-253-2021>
- 718 Thibeault, J. M., & Seth, A. (2014). Changing climate extremes in the Northeast United States: observations and
719 projections from CMIP5. *Climatic Change*, *127*(2), 273-287. <https://doi.org/10.1007/s10584-014-1257-2>
- 720 Tokarska, K. B., Stolpe, M. B., Sippel, S., Fischer, E. M., Smith, C. J., Lehner, F., et al. (2020). Past warming trend
721 constrains future warming in CMIP6 models. *Science Advances*, *6*(12), eaaz9549.
722 <https://doi.org/10.1126/sciadv.aaz9549>
- 723 Xie, S. P., Deser, C., Vecchi, G. A., Collins, M., Delworth, T. L., Hall, A., et al. (2015). Towards predictive
724 understanding of regional climate change. *Nature Climate Change*, *5*(10), 921-930.
725 <https://doi.org/10.1038/nclimate2689>
- 726 Zhang, X., Alexander, L., Hegerl, G. C., Jones, P., Tank, A. K., Peterson, T. C., et al. (2011). Indices for monitoring
727 changes in extremes based on daily temperature and precipitation data. *Wiley Interdisciplinary Reviews:*
728 *Climate Change*, *2*(6), 851-870. <https://doi.org/10.1002/wcc.147>
- 729 Zhang, X., Hegerl, G., Zwiers, F. W., & Kenyon, J. (2005). Avoiding inhomogeneity in percentile-based indices of
730 temperature extremes. *Journal of Climate*, *18*(11), 1641-1651. <https://doi.org/10.1175/jcli3366.1>
- 731